Biomaterials 281 (2022) 121322

Contents lists available at ScienceDirect

Biomaterials

journal homepage: www.elsevier.com/locate/biomaterials

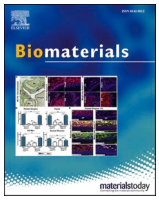

Recent development of metal-organic framework nanocomposites for biomedical applications

Xueying Ge [a], Raymond Wong [b], Anee Anisa [a], Shengqian Ma [a,*]

[a] Department of Chemistry, University of North Texas, 1508 W Mulberry St, Denton, TX, 76201, United States
[b] Department of Cell and Molecular Biology, University of South Florida, 4202 E. Fowler Avenue, Tampa, FL, 33620, United States

ARTICLE INFO

Keywords:
Metal-organic frameworks (MOFs)
Nanoparticles
Cancer therapy
Biomedical application
Nanocomposites

ABSTRACT

Albeit metal-organic framework (MOF) composites have been extensively explored, reducing the size and dimensions of various contents within the composition, to the nanoscale regime, has recently presented unique opportunities for enhanced properties with the formation of MOF-based nanocomposites. Many distinctive strategies have been used to fabricate these nanocomposites such as through the introduction of nanoparticles (NPs) into a MOF precursor solution or vice versa to achieve a core-shell or heterostructure configuration. As such, MOF-based nanocomposites offer seemingly limitless possibilities and promising solutions for the vast range of applications across biomedical disciplines especially for improving *in vivo* implementation. In this review, we focus on the recent development of MOF-based nanocomposites, outline their classification according to the type of integrations (NPs, coating materials, and different MOF-derived nanocomposites), and direct special attention towards the various approaches and strategies employed to construct these nanocomposites for their prospective utilization in biomedical applications including biomimetic enzymes and photo, chemo, sonodynamic, starvation and hyperthermia therapies. Lastly, our work aims to highlight the exciting potential as well as the challenges of MOF-based nanocomposites to help guide future research as well as to contribute to the progress of MOF-based nanotechnology in biomedicine.

1. Introduction

Metal-organic frameworks (MOFs) represent an emerging class of materials, featuring periodic coordination networks that are bridged between organic linkers and metal-containing nodes and can be designed into various topologies through reticular synthesis [1,2]. Given the unique characteristics of the crystalline structures exhibited by MOFs, such as large specific surface areas and high porosity, these materials are especially advantageous as carriers in achieving high drug loading efficiency facilitated by host-guest interactions [3]. Notably, the highly ordered porous structures of these framework materials provide enormous opportunities for versatile functionalization as promising platforms tailored for specific applications, such as catalysis, imaging, and cancer therapy [4–8]. Moreover, via pre-functionalizing [9] and post-synthetically modifying [10–12] the metal nodes and the organic linkers, MOFs can be rendered with distinctive magnetic [13], electronic [14], catalytic [15] and optical properties [16]. The use of the rare-earth elements [17] and transition metals (e.g., Co, Mn, Fe, *etc.*) as a node to construct MOFs makes them hold promise for application in catalysis [18], imaging [7], and sensing [19].

It has recently been explored for the employment of MOFs as host matrices to integrate various functional materials, such as NPs [20–22], bioentities [23,24], and polymers [25,26], which give rise to composites with enhanced or new properties as compared with their parent frameworks [27]. Among these MOF composite materials, the size of the host MOFs and/or the guest functional materials can be further reduced to the nanoscale regime to afford metal-organic framework nanocomposites [28]. These MOF nanocomposites are more compatible for bio-circulation, acting as efficient nanocarriers to deliver agents for bio-applications [4,29]. By incorporating various functional NPs, such as Au [30,31], Fe_3O_4 [32], quantum dots [33] and upconversion NPs [34], into MOF structures, it enables the nanocomposites to preserve the properties originating from the versatile crystalline and porous structures of MOFs, and also to sustain the unique biomimetic catalytic, optical-electrical, and magnetic properties of the NPs. Furthermore, the synergistic effect from the integration of these materials can evoke new chemical and physical properties.

To date, NPs incorporated within MOFs for catalytic applications

* Corresponding author.
E-mail address: Shengqian.Ma@unt.edu (S. Ma).

https://doi.org/10.1016/j.biomaterials.2021.121322
Received 16 September 2021; Received in revised form 1 December 2021; Accepted 12 December 2021
Available online 15 December 2021

have been extensively studied and summarized [20,22,35–37]. Many reports have also reviewed about MOF composites for bio-applications such as biomimetic catalysis [38–41], drug delivery [42–45], bio-imaging [29,46], and cancer therapy [4,27,47]. Distinct from previous reviews, our work herein focuses on the recent progress of MOF-based nanocomposites that are classified in accordance with the type of integrations, such as various NPs integrated into MOF structures, coating or doping nanoMOFs by SiO_2, graphene, and metal polyphenol networks, and different MOF-derived nanocomposites (Fig. 1). Further, we highlight their potential for biomedical applications including biocatalytic, photo, chemo, sonodynamic, starvation and hyperthermia therapies. With the emergence of nanocomposites in this field, attention should be drawn to the potential opportunities and challenges of these nanomaterials so as to facilitate their advancements in design and functionalities as well as to contribute to the development of their potential utility for biomedical employment.

2. NPs/MOFs

2.1. Synthetic methods of NPs/MOFs

Given the inherent property of high surface energy, NPs are thermodynamically unstable and susceptible to aggregation, thus resulting in the loss of magnetism [48], catalytic [49] and optical activity [50]. Nevertheless, this limitation can be circumvented with the use of MOFs as their multiple coordination sites and well-defined pore structure can stabilize NPs by providing spatial confinement and preventing them from aggregation. Moreover, NPs/MOF nanocomposites exhibit a synergistic effect and thereby affording enhanced properties. As indicated by the emerging literatures, many studies have explored the development of a diverse array of synthetic methods to integrate NPs into MOFs [20,35,51]. One such approach is through the "ship-in-bottle" strategy, in which the MOF is introduced into a solution containing a metal precursor, followed by the formation of NPs inside or on the surface of the MOFs. The "bottle-around-ship" is another approach and can be achieved by introducing prepared NPs as seeds or nucleation centers into a MOF precursor solution and growing the MOF layer around NPs. However, the resulting NPs@MOF nanocomposites may occasionally preserve the shape of pristine NPs, and subsequently, lead to low Brunauer-Emmett-Teller (BET) surface areas (S_{BET}). Originating from the "bottle-around-ship" approach is the "one-pot" strategy by which the pre-synthesized NPs are introduced into the MOF precursor solution, wherein the NPs can be integrated both inside and outside of the nanocomposites because the growth of MOFs is not along with the NPs. The "layer-by-layer" approach represents another strategy, which grows MOFs around the NPs layer by layer to enhance the porosity properties of the nanocomposites. Both the "bottle-around-ship" and "layer-by--layer" methods can be further supplemented with surface functional

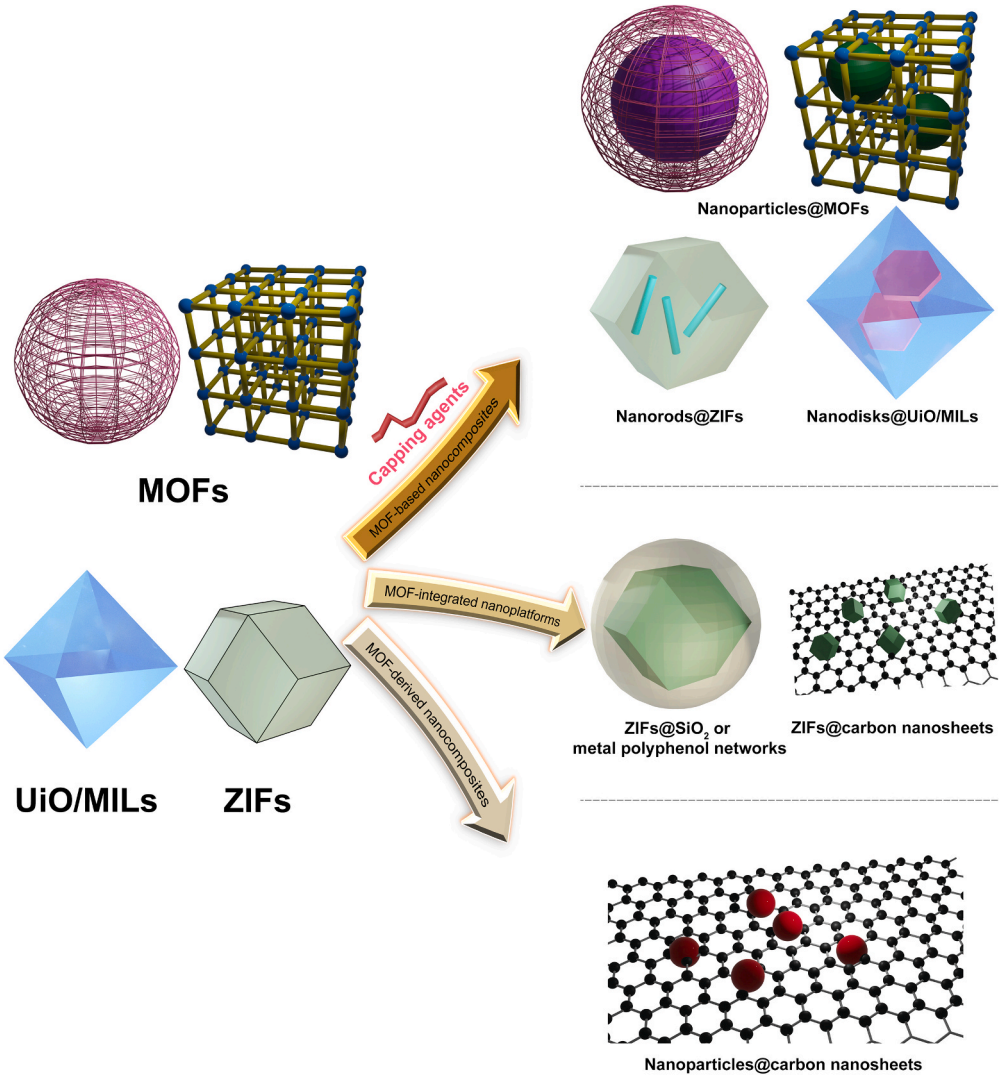

Fig. 1. Schematic diagram of various designs in the formation of MOF-based nanocomposites.

groups, such as polyvinylpyrrolidone (PVP) [36,52–55], hexadecyl trimethyl ammonium bromide (CTAB) and carboxylic acids (*i.e.* mercaptoacetic acid (MAA)", poly(acrylic acid) (PAA) and 3, 4-dihydroxyhydrocinnamic acid) [56–58,110], which can be used to decorate NPs in assisting with the assembly of MOFs in a relatively well-controlled manner as these functional groups can make the NPs water-dispersible. Lastly, the synthesized NPs and MOFs can be physically mixed via sonication. To this end, the NPs can be attached onto the MOF structures via physical adsorption and/or electrostatic interactions [59,60] (Fig. 2). With various NPs and strategies for constructing nanoparticle/MOF composites, their properties could be tailored to improve therapeutic effect for numerous biomedical applications including catalysis, drug delivery, and cancer therapy.

2.2. Biomedical applications of NPs/MOFs

Enzyme-mimic active centers such as tetrakis(4-carboxyphenyl) porphyrin) (TCPP) as a heme-like ligand [61] and iron as an active site can be used to construct MOFs in facilitating their catalytic potential. Although MOFs constructed from TCPP and/or iron have received much attraction in the last decades, their employment in bio-catalytic application is still hindered by their limited active sites and poor mechanical, thermal, and chemical stabilities [62]. As such, substantial efforts have focused on the integration of NPs, especially nanozymes like Au, Pt, Pd, Fe_3O_4, into MOFs to offset the weakness of pristine MOFs and to improve their catalytic performances [63]. The fabrication of such nanocomposites can be employed for reactive oxygen species applications such as photodynamic therapy (PDT). When upconversion NPs (UCNPs) are combined with MOFs, the nanocomposites can shift the excitation wavelength to "therapeutic window" (650–1100 nm) for deeper tissue penetration, ultimately enhancing photodynamic therapeutic effect. Notably, other studies have shown promising results for the use of Au NPs to construct MOF-based nanocomposites for photothermal therapy (PTT) due to their surface plasmon resonance (SPR) attributes. Acquisition of thermal properties of NPs such as Fe_3O_4 are commonly known to induce the hyperthermia effect under the irradiation of alternative magnetic field (AMF), enabling Fe_3O_4/MOF nanocomposites with hyperthermia treatment. To date, progress in the latest advances of nanomaterials, such as noble metals, iron oxide NPs (IONPs), UCNPs, cerium oxide NPs, quantum dots, and persistent luminescent NPs have shown advantageous opportunities for biomedical applications. In this content, we summarize various nanoparticle-MOF integrations to detail their potential utilization.

2.2.1. Noble metal NPs/MOFs

Encapsulating noble metal NPs such as Au, Pt, Pd NPs into MOFs presents many advantages for biomedical utilization as MOF-based carriers offer structural stability for spatial confinement in preventing NPs from aggregation.

2.2.1.1. Au NPs. AuNPs due to their chemically inert property have been utilized in the biological catalysis field [64–67]. Such nanomaterials with catalytic capabilities are known as "nanozymes". Growing interest has led to considerable efforts in mimicking natural enzymes using AuNPs as their catalytic potential has been extensively studied through the support of activated carbons, metal oxides, mesoporous materials, and zeolites [68]. As such, MOFs present pivotal advantages as platforms to immobilize enzymes [69] and nanozymes, further amplifying the performance of the catalysis system [70]. Given the versatile spatial distribution of metal ions and organic linkers of MOFs, the framework could be rationally designed with nanosized channels and cavities, exhibiting many similarities to those found in

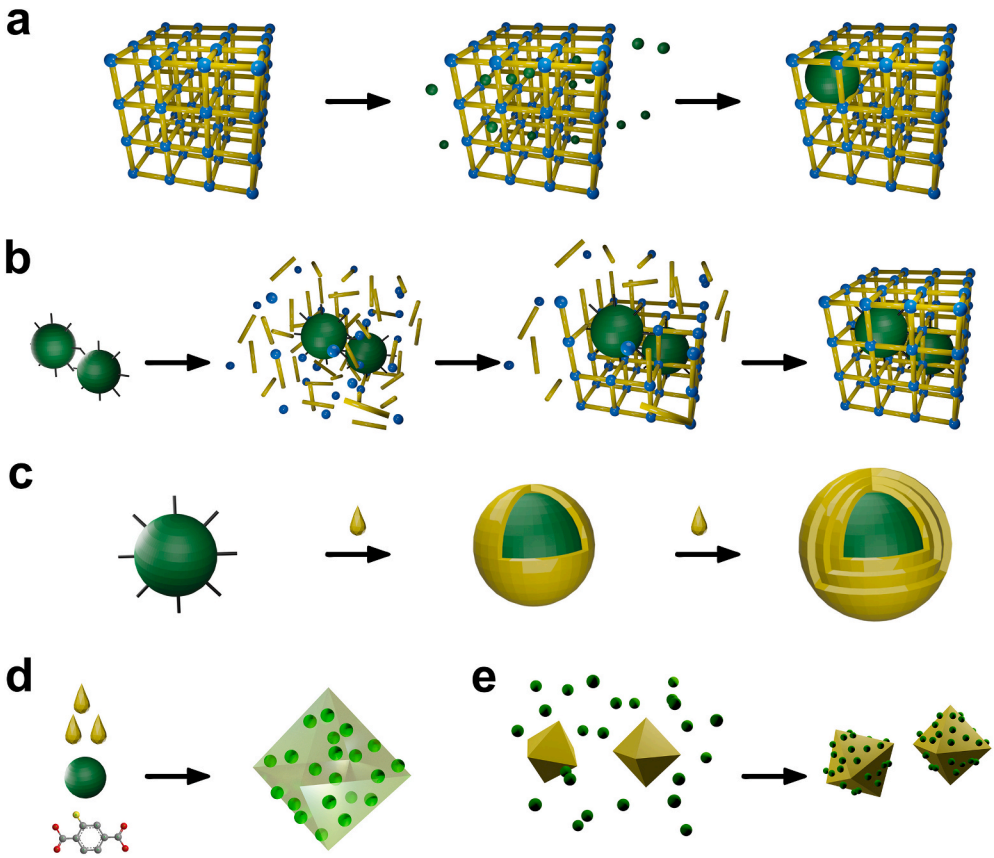

Fig. 2. Schematic diagram of different synthetic methods to integrate NPs into MOFs: (a) "ship-in-bottle" strategy; (b) "bottle-around-ship" strategy; (c) "layer-by-layer" strategy; (d) "one-pot" strategy; (e) mixing strategy.

other carriers. In the last decades, many groups have reported loading Au NPs into MOFs [30,36,71–73]. For instance, Wei's group designed a nanozyme, AuNPs@MIL-101 by *in-situ* growing Au NPs into Material of Institute Lavoisier (MIL)-101, showing integrative properties of peroxidase (POD)-mimicking and surface-enhanced Raman scattering (SERS) [74] (Fig. 3A). Further, glucose oxidase and lactate oxidase were incorporated into the AuNPs@MIL-101 nanocomposites which demonstrated the detection of lactate and glucose through SERS. The prepared nanocomposite with the enzyme immobilization displayed an excellent sensitivity and a signal amplification towards lactate and glucose via SERS signal with a detection limit of 5.0×10^{-6} M and 4.2×10^{-6} M, respectively. Porphyrin-based two-dimensional MOFs have also been successfully employed as biomimetic enzymes [75]. However, one potential limitation is that they are restricted to mimicking the enzymatic activities of only one type of enzyme. As such, Zhang and co-workers have fabricated a multienzyme biomimetic cascade system by integrating Au NPs into 2D metalloporphyrinic MOF nanosheets with POD-like activity using the "ship-in-bottle" approach to reduce $HAuCl_4$ with reducing agent in the existence of Cu-TCPP(Fe) [76]. Furthermore, Paul et al. encapsulated both gold NPs and glucose oxidase into MOF pores, constructing an attractive nanocomposite that achieves a low detection limit of 50 nM for glucose [64]. Feng et al. designed a sandwich electrochemical immunosensor to detect prostate-specific antigen based on Fe-MIL-88B–NH_2 coated with gold NPs and functionalized with labelling antibodies [77].

Free electrons found in Au NPs create a coherent oscillation associated with the induction produced by the oscillating electromagnetic field of the incident light. A surface plasmon resonance (SPR) is produced when the maximum amplitude of the oscillation is attained at a distinct frequency [78]. The localized SPR spectrum of Au NPs can expand to near-infrared region via controlling the morphology, size, and shape. Given the SPR phenomenon that Au NPs produces, Au NPs

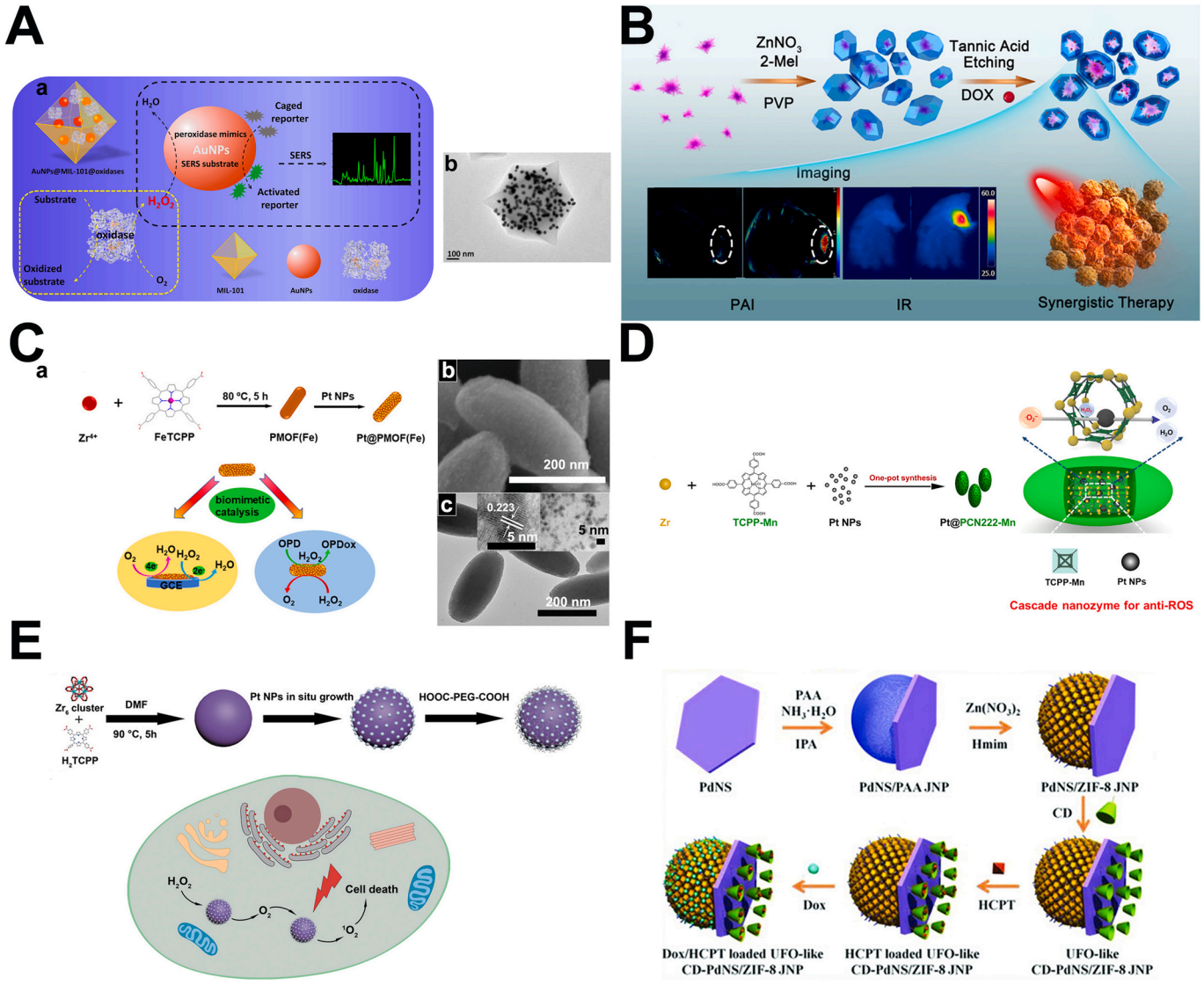

Fig. 3. (A) (a) Schematic illustration of AuNPs@MIL-101@oxidases for efficient enzymatic cascade reactions; (b) TEM image of AuNPs@MIL-101 [74]. Reproduced with permission. Copyright 2017, *ACS nano*. (B) Schematic illustration for the fabrication process, IR/Photoacoustic imaging (PAI) effects, and synergistic anticancer therapy of Au@MOF-DOX [87]. Reproduced with permission. Copyright 2019, *Nano Lett.* (C) (a) Preparation of Pt@PMOF(Fe) and biomimetic Catalysis of Pt@PMOF (Fe); (b) Scanning electron microscope and (c) TEM images of Pt@PMOF(Fe) [93]. Reproduced with permission. Copyright 2020, *ACS Appl. Mater. Interfaces.* (D) Synthetic procedure of Pt@PCN222–Mn and constructing a cascade nanozyme for anti-ROS therapy by embedding Pt NPs inside PCN222–Mn MOF. Nanoscale proximity of catalytic active sites promotes the cascade reactions [95]. Reproduced with permission. Copyright 2020, *Sci. Adv.* (E) Schematic illustration of the preparation process and enhanced photodynamic effect of PCN-224-Pt [96]. Reproduced with permission. Copyright 2018, *ACS nano*. (F) Schematic diagram of preparing UFO-like CD-PdNS/ZIF-8 JNPs [1]. Reproduced with permission. Copyright 2018, *Adv. Funct. Mater.*

possess significant potential for application in PTT. Moreover, the photothermolysis properties of gold also present advantages for X-ray computed tomography as a contrast agent. Shang et al. designed a carboxylic acid-functionalized Au nanorod@MIL-88(A) nanocomposite for multimodality diagnoses of glioma. This nanocomposite as a contrast agent can be employed in computed tomography (CT), photoacoustic and magnetic resonance imaging [80]. Moreover, Zhang et al. used layer-by-layer methods to grow NH_2-MIL-101 shells around a gold nanostar, followed by post-modifications with a ZD2 peptide [81]. The constructed nanocomposites demonstrated photothermal therapeutic effects towards triple-negative breast cancer. Tang's group designed Au nanorod@MOF nanocomposites by growing a zeolitic imidazolate framework (ZIF)-8 layer around PVP-functionalized Au nanorods via "bottle-around-ship" method, followed by drug loading into the nanocomposites. Under 808 nm laser irradiation, the drug loaded nanocomposites showed chemo and photothermal therapeutic effects [82]. Furthermore, Au NPs as nanozymes have displayed great progress in mimicking catalase (CAT)-like activity. Ma et al. embedded Au NPs on ZIF-8 surface along with the encapsulation of chlorin e6 (Ce6), attaining efficient PDT [83]. Zeng et al. also reported an effective strategy in constructing a multimodal cancer therapeutic nanoplatform for combined PTT, PDT, and chemotherapy functionalities [84]. Likewise, their strategy involves a "bottle-around-ship" method to grow porphyrin-based MOF shells around CTAB-functionalized Au nanorods, followed by loading camptothecin. Under 808 nm laser irradiation, the nanocomposites displayed an enhanced hyperthermia effect and an increased drug release rate. Under 660 nm light-emitting diode (LED) irradiation, the nanocomposites produced reactive oxygen species (ROS). It should also be noted that when the nanocomposite is irradiated under 606 nm and 808 nm, remarkable synergistic efficiency was displayed in killing the tumor cells both *in vitro* and *in vivo*. In another study, He et al. designed Au@$Cu_3(BTC)_2$ nanocomposites for chemo-photothermal and Raman imaging therapy by growing MOF ($Cu_3(BTC)_2$) shells around Raman reporter molecule (4-mercaotobenzoic acid)-functionalized Au NPs, followed by post-modifications with aptamer and doxorubicin (DOX) loading [85]. In order to acquire deep tissue penetration, NIR is always used to irradiate the biological system. Recently, second-NIR region (1000–1350 nm) laser-induced PTT has shown stronger tumor therapeutic effects due to the deeper penetration depth and larger maximum permissible exposure [86]. Deng et al. fabricated a yolk-shell nanocomposite, Au nanostar@ZIF-8, by growing a ZIF-8 shell around PVP-modified Au NPs via "bottle-around-ship" methods. This nanocomposite can absorb the light which is located at the NIR-II region due to the presence of the Au nanostar. Further, DOX was loaded into the yolk-shell nanocomposites with a loading content of 29%. Under 1064 nm laser irradiation, the temperature of the yolk-shell nanocomposite solution could be reached to almost 100 °C and the photothermal conversion efficiency of yolk-shell nanocomposite was found to be 48.5%. Furthermore, the combined chemo-photothermal effect was successful in inhibiting tumor growth [87] (Fig. 3B).

2.2.1.2. Pt NPs. In addition to Au NPs, Pt NPs have also been demonstrated to be one of the most effective catalysts [88] with the enzymatic capabilities of superoxide dismutase (SOD), and POD, CAT. As aforementioned, MOFs can be utilized as carriers for NPs of which they can help support Pt NPs in avoiding aggregation [89,90]. The modifications on the outer surface of Pt@CuMOF with aptamer, hemin, and glucose oxidase have shown to attribute to signal amplifications in cascade reaction. In this study, Pt@CuMOF nanocomposites were synthesized via "ship-in-bottle" approach by embedding Pt NPs on the CuMOF framework [91]. Aside from building MOFs with the ligand of 2-aminoterephthalic acid as discussed above, several studies have used TCPP with a heme-like center as a ligand to construct porphyrin-based MOFs, enabling MOFs with biomimetic activity. Chen et al. reported the growth of Pt NPs on the Cu-TCPP(Fe) nanosheet through the "ship-in-bottle" strategy, showing an increased catalytic activity compared with pristine Pt NPs [92]. In this study, a photochemical reduction method was developed in synthesizing hybrid nanosheets via liquid growth of Pt NPs on MOF nanosheets. High resolution transmission electron microscopy (HRTEM) images confirmed the dispersion of Pt NPs supported by the MOFs through lattice spacing of Pt (111) and Pt (200). These hybrid nanosheets displayed a favorable catalytic affinity for hydrogen peroxide (H_2O_2) with a linear relationship of H_2O_2 from 2 μM to 0.1 mM and a detected concentration as low as 0.357×10^{-6} M. Additionally, the hybrid nanosheets could also detect the concentration change of glucose from 2 μM to 0.2 mM with a detection limit of 0.994×10^{-6} M, suggesting its strong potential use as a sensitive sensor compared with other nanomaterials. Ling et al. also used the "ship-in-bottle" approach to embed Pt NPs onto the PMOFs structure constructed by metalloporphyrin (FeTCPP) and Zr^{4+} ions. The designed Pt@PMOF(Fe) exhibited CAT-like and POD-like activities. The substrate, o-phenylenediamine (OPD) was used to investigate the POD-like property. Furthermore, the Michaelis constant of OPD for Pt@PMOF(Fe) was 0.866 mM, which is approximately 10 times smaller than the pristine PMOF, indicating that the presence of Pt NPs can enhance the catalytic activity. Given the enzyme-mimetic properties of Pt NPs and FeTCPP, an enhanced electrochemical signal was also found when Pt@PMOF was modified on an electrode [93] (Fig. 3C). Furthermore, Li et al. designed a sandwich-like nanozyme MOF/Pt/MOF, via a physical mixture of two pre-synthesized PVP-modified Pt NPs and MOF materials, followed by encapsulating another MOF layer outside of MOF@Pt nanocomposites to detect exosome miRNA with a detection limit of 0.29 fM [94].

Excessive ROS production is often associated with many inflammatory diseases such as glomerulonephritis, hepatitis, and inflammatory bowel disease (IBD). While some nanozymes with multiple-ROS-scavenging capabilities have been employed through *in vivo* therapies, many of these systems are hindered by their own properties such as a lack of multiple active sites, low specific surface area, and relatively moderate biocompatibility. As such, the approach of incorporating MOFs as carriers can help overcome these limitations as their robust and versatile features in structural design and synthetic capabilities are widely recognized in biomedical applications. In one study, Liu et al. constructed an enzyme-like cascade system via one-pot approach for anti-ROS therapy by introducing Mn(III) porphyrin with SOD-like activity and Pt NPs with CAT-like activity, within a nanoscale Zr-based porous coordination network (PCN)-222, ultimately achieving Pt@PCN-222-Mn [95]. Loaded with 6% of Pt NPs, this nanocomposite showed superior catalytic efficiency in both SOD- and CAT-like activities *in vitro* in comparison to free Pt NPs and physical mixture of Pt NPs and PCN-222-Mn. Further, *in vivo* mice experiments found that Pt@PCN-222-Mn synergistically increased ROS-scavenging activity and thereby, providing an effective method in protecting the mice from ROS-related IBD. As such, this work demonstrated that the one-pot approach is a favorable strategy in constructing an integrated nanozyme with multifunctional active sites for potential clinical use in cancer therapy (Fig. 3D). Alternatively, Zhang et al. reported an *in-situ* growth approach through the reduction of H_2PtCl_6 to immobilize Pt nanozymes onto the formed PCN-224 framework to generate reactive singlet oxygen ($^1O_2$), and thereby, achieving CAT-like activity. After exposure to light irradiation, no significant therapeutic effect for PCN-224 was found due to the hypoxia effect. This further provides evidence that Pt NPs used as nanozymes, possess CAT-like properties and thereby, result in the formation of more $^1O_2$ to enhance PDT [96] (Fig. 3E). In addition to their work, Wu's group fabricated a sandwich-like structure, MOF/NPs/MOF, called P@Pt@P–Au-FA where PVP-coated Pt NPs were embedded between the shell layers of PCN [97]. This acquired shell structure (P@Pt@P) was further modified with the confinement and dispersion of ultrasmall "naked" Au NPs and with post-modification of folic acid (FA) on the outer shells of the nanocomposite. Given the catalytic properties of these NPs, this nanocomposite exhibited GOx-mimicking and

CAT-mimicking activities, originating from ultrasmall Au NPs, and Pt NPs, respectively. Moreover, several mice tumor experiments demonstrated that the prepared P@Pt@P–Au-FA nanocomposite achieved good tumor cytotoxicity effects in both ambient and hypoxic conditions due to the production of O_2 resulting from the decomposition of H_2O_2 catalyzed by Pt NPs. This nanocomposite also exhibited superior therapeutic efficiency in comparison with other reaction platforms.

2.2.1.3. Pd NPs. Zhang et al. prepared a Pd nanosheet-based Janus nanocomposite via selectively growing ZIF-8 along with the polyacrylic acid-functionalized Pd nanosheet, followed by modifying cyclodextrin, and loading DOX. Ultimately, their design afforded synergistic dual drug chemo and photo therapies in NIR-II windows [1] (Fig. 3F).

2.2.2. Upconversion NPs (UCNPs)

Nanomaterials like UCNPs have shown promising potential in converting NIR light to visible light for the excitation of photosensitizers (PSs) to enhance penetration depth by using the "therapeutic window" (650–1100 nm) as excitation wavelength [98]. Moreover, aggregation of UCNPs can also be prevented to a certain degree by the covalent binding or physical attachment of PSs onto UCNPs. However, such surface modification typically is a difficult and tedious process. Furthermore, under long-term light exposure, PSs leakage and/or photodecomposition may be encountered with the use of such surface modification. In maximizing the PDT efficiency, this configuration is also not favorable especially in the adsorption process of oxygen onto UCNPs. Therefore, MOFs are excellent candidates for carriers in controlling the access and contact of the guest and preventing their aggregation. Cai et al. used the "bottle-around-ship" approach in assembling a core-shell structure, UCNPs/MB@ZIF-8 by introducing pre-synthesized UCNPs into the MOF precursor solution and later surface-modified with CAT. The incorporation of CAT can enhance the production of O_2 by catalyzing endogenous H_2O_2. Moreover, the $^1O_2$ was generated under NIR light irradiation through the fluorescence resonance energy transfer (FRET) between MB and UCNPs, displaying high efficiency in PDT against hypoxic tumors [99]. Since MOFs are exceptional candidates for O_2 storage [100], the use of ZIF-90 materials as a carrier to store oxygen for PDT is reported by Xie et al. [101]. In this study, a multimodal drug carrier, URODF, was designed and optimized with pH-controlling as well as O_2-storing capabilities. UCNPs were used as dual-modal imaging agents and encapsulated into the mesoporous silica NPs, further loaded with rose bengal and coated outside with ZIF-90. Given the aldehyde group on the ligand of ZIF-90, NH_2-poly (ethylene glycol) functionalized folic acid and DOX can be linked outside of the ZIF-90 shells. In a low pH microenvironment, the disassembly of ZIF-90 improved the release rate of O_2 and DOX. With NIR light exposure, UCNPs and MB transferred energy along with the release of O_2 and DOX, resulting in an enhanced synergetic therapy and thus, overcoming tumor hypoxia. Ling et al. also used the "bottle-around-ship" approach to grow a ZIF shell around PVP-modified UCNPs to construct UCMOF. Further, DOX was covalently attached to UCMOF, followed by loading of 5-fluorouracil (5-FU) into the mesopores. This designed nanocomposite possesses the capabilities to achieve synergistic cancer treatment [102].

UCNPs@MOF nanocomposites can also be used to construct fluorescent probes. Hao et al. designed a hybrid chiral nanostructure by coating a ZIF-8 layer onto the PVP-functionalized UCNPs nanodisks, followed by a decoration of chiral NiSx NPs onto the MOF shells for ROS quantitative monitoring [103]. Chiral NiSx NPs with strong chiroptical activity can prevent the background circular dichroism signals of biological matrices. Furthermore, the upconversion luminescence (UCL) peak of nanocomposites was quenched by the CD peak of NiSx NPs at 540 nm. However, the UCL peak of UCNPs at 660 nm was nearly identical. When the H_2O_2 concentration was within 0.05–20 μM, the intensity ratio of UCL at 660 nm–540 nm displayed a linear response with a detected concentration as low as 0.037 μM. The detection range of the CD signal at PCS-460-010 cells was 0.18–10.2 μM with a detected concentration as low as 0.09 μM. Furthermore, the *in vivo* ROS detection was also shown in a mouse experiment (Fig. 4A).

Porphyrin-based MOFs constructed by porphyrin ligands have attracted much attention for their use in light-harvesting systems as it can avoid self-quenching. He et al. prepared DNA-assembled core-satellite nanocomposites by conjugating UCNPs around the porphyrin-based MOF NPs via DNA oligonucleotides, achieving PDT potential [105]. However, this strategy requires the control of the NPs' valency and extra purification process is needed to obtain the core-satellite nanocomposites. With this regard, Yan and the co-workers designed a Janus structure by growing Zr-based porphyrin MOFs around PVP-modified UCNPs NPs (UMOF) [98]. Due to the preferable binding of PVP with the (001) facet of the UCNPs, the growth of MOFs was only along the (001) facet of the UCNPs forming the Janus structure. The photoluminescent quantum yield of the Janus nanocomposites was 0.2% under the 980 nm laser irradiation. The singlet oxygen sensor green (SOSG) presented an opportunity for this nanocomposite to produce $^1O_2$, which laid the foundation for PDT potential under NIR irradiation. In addition to Yan's work, Zhao's group reported 808 nm NIR light-triggered Janus nanocomposites by growing porphyrin-based MOFs around the Nd^{3+}/Yb^{3+}/Er^{3+}-based UCNPs [106]. The nanocomposite can generate $^1O_2$ under 808 nm laser to induce mitochondria-target PDT effects. Moreover, the nanocomposite irradiated by 808 nm can prevent from subsequent laser-irradiation-triggered overheating effects due to the biological tissue's minimal absorption, demonstrating that this Janus nanocomposite can overcome this current limitation of PDT treatments. Recently, Yuan's group also reported a facet-selective nanocomposite by growing two-dimension MOFs around PVP-modified UCNPs, further promoting the development of nanocomposites for potential bio-applications [107]. PVP-modulated synthetic methods can only be formed in the Janus structure for the UCNPs and MOF, which hides the energy transfer between the UCNPs and MOF. In addition to their work, Yan and the co-workers proposed a method in improving this design by changing PVP-mediations to citrate acid-mediations. This strategy can form a core-shell structure to enable the growth of MOF layers around the UCNP cores. Additionally, a hypoxia-triggered prodrug, tirapazamine was loaded into MOF pores. Ultimately, the drug loaded UCNP@MOF core-shell structure displayed improvements to cancer therapy both *in vivo* and *in vitro* by combining PDT and chemotherapy together [108] (Fig. 4B).

Moreover, numerous studies employ PVP which is a capping agent that is used to functionalize UCNPs, assisting in the assembly of the MOF nanocomposite. However, the prevalence of PVP may also hinder the potential use of nanocomposites in future applications. As such, Yuan et al. proposed an *in-situ* self-assembly methods to construct MOF/UCNPs nanostructures by paving MOF with UCNPs without introducing capping agents. Acid-treated UCNPs with a positive charge can be attracted by the negative charged University of Oslo (UiO)-66-NH_2 via electrostatic force. Subsequently, the surface of the MOF can be fully covered by UCNPs. Moreover, the obtained MOF/UCNPs nanocomposites can be further modified to a "sandwich-like structure" by epitaxially growing another MOF layer. Sandwich-like nanocomposites have shown potential in drug delivery and PDT applications under 980 nm laser irradiation [60] (Fig. 4C). Furthermore, Li et al. used the same self-assembly methods to pave UiO-68-NH_2 with Nd^{3+}-sensitized UCNPs with co-loading of Ce6 and rose bengal, achieving amplified PDT effects under 808 nm laser irradiation and avoiding overheating limitations [109] (Fig. 4D).

Based on the growth mechanism of MOFs, carboxylic acid ligand can be used to decorate the desired encapsulated-NPs, assisting the assembly of MOFs. With this regard, the carboxylic acid-functionalized NPs may regard as the coordination group together with the organic ligand to coordinate with metal ions or clusters in forming MOF-based nanocomposites. Liu et al. utilized a ligand exchange method to switch the hydrophobic ligand-functionalized UCNPs to carboxylic acid-

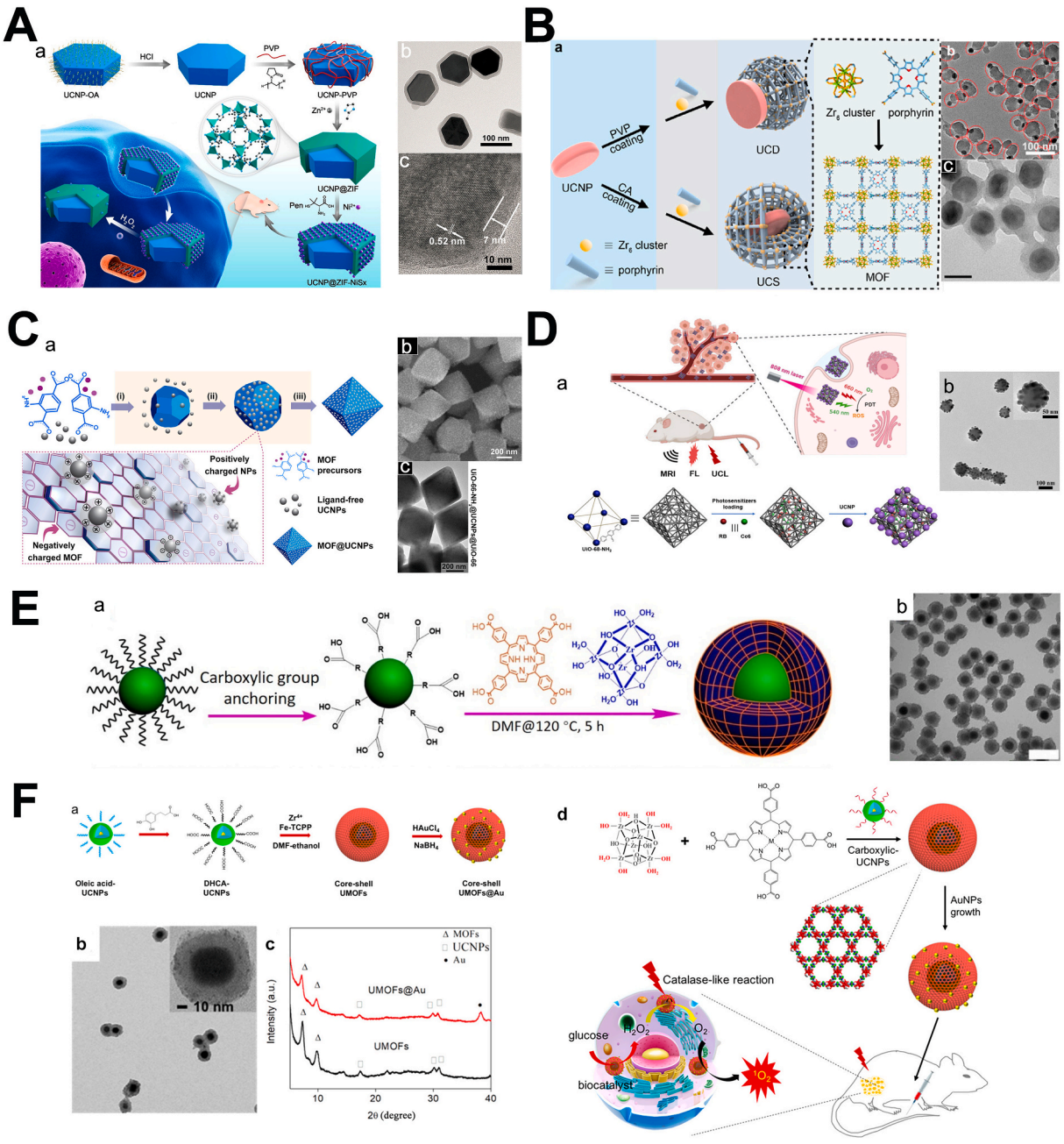

Fig. 4. (A) (a) ROS detection using UCNP@MOF-NiSx nanoassemblies; (b) TEM and (c) HRTEM images of the UCNP@ZIF nanostructure [103]. Reproduced with permission. Copyright 2019, *J. Am. Chem. Soc*. (B) (a) Schematic illustration of the synthesis of UCDs and UCSs through the conditional surface engineering of UCNPs; (c) TEM image of UCSs [108]. Reproduced with permission. Copyright 2020, *J. Am. Chem. Soc*. (b) TEM image of UCMOFs [98]. Reproduced with permission. Copyright 2017, *J. Am. Chem. Soc*. (C) (a) Schematic illustration of the fabrication of UCNPs and MOF nanocomposites; (b) SEM images of the obtained UiO-66-NH_2 and ligand-free $NaYF_4$:Yb/Er nanocomposites; (c) TEM image of MOF@NPs@MOF core–shell–shell sandwiched nanocomposites [60]. Reproduced with permission. Copyright 2018, *J. Am. Chem. Soc*. (D) (a) Schematic illustration of the fabrication process of the core–satellite CR@MUP theragnostic nanoplatform and its operation for imaging-guided PDT; (b) TEM image of CR@MUP [109]. Reproduced with permission. Copyright 2020, *Nano Res.* (E) (a) Schematic illustration of grafting ZrMOF on a single nanocrystal; (b) TEM image of UCNP@ZrMOF NPs [110]. Reproduced with permission. Copyright 2019, *J. Am. Chem. Soc*. (F) (a) Scheme of the synthesis of core–shell UMOFs@Au NPs; (b) TEM images and (c) X-ray diffraction (XRD) patterns of UMOF@Au; (d) scheme of core–shell UMOFs@Au NPs for synergistic cancer therapy driven PDT through cascade catalytic reactions [34]. Reproduced with permission. Copyright 2020, *J. Am. Chem. Soc*.

functionalized UCNPs. Further, carboxylic acid functionalized-UCNPs were coated by ZrMOF with a TCPP ligand via an Ostwald ripening process, constructing UCNP@ZrMOF. Though, it should be noted that this process can only be used to graft a single nanoparticle. As detected by SOSG, UCNP@ZrMOF nanocomposites can produce $^1O_2$ under 980 nm laser irradiation [110] (Fig. 4E). In addition to this work, Chen and his co-workers designed a biocatalysts nanoplatform, UMOF@Au, by integrating ultrasmall Au NPs with core-shell UCNP@ZrMOF whose ligand is Fe-TCPP [34]. The integration of AuNPs dispersed on the MOF matrix can consume glucose to generate H_2O_2. Therefore, H_2O_2 can be decomposed to oxygen, while $^1O_2$ is produced by activating UMOF under 980 nm laser irradiation, strongly demonstrating that the nanocomposites have NIR-induced synergistic cascade catalysis driven by PDT effects (Fig. 4F). These UCNPs@MOF nanocomposites primarily focused on the single FRET technique. Recently, Lei's group proposed a dual FRET strategy by one excitation to achieve NIR-responsive drug

delivery [111]. The azobenzene-based MOF shell was *in situ* grown around the carboxylic acid functionalized-UCNPs core and loaded with a photo-responsive prodrug and 10-hydroxycamptothecin. Under NIR excitation, two UCL were sensitized by the inner UCNPs core, and the outer MOF layer changed its conformation through *trans-cis* photoisomerization under one UCL, subsequently causing an anticancer drug release. Furthermore, another UCL led to the photo-cleavage of the prodrug.

Many groups have built multimodal cancer therapeutic nanoplatforms to achieve an enhanced therapy effect. In one study, Zhang et al. encapsulated UCNPs, Ag_2S, and Ag_2Se NPs and DOX into ZIF-8 frameworks via one-pot method, ultimately achieving a combination of chemotherapy and PDT [112]. Shi et al. designed a heterodimer nanocomposite by growing porphyrin-based MOFs around PVP-functionalized UCNPs [113]. Then, titanium dioxide NPs were covered on the surface of the UCNPs@MOF nanocomposites since the use of titanium dioxide as a photocatalyst semiconductor for cancer therapy presents advantages such as low toxicity, and good biocompatibility and chemical stability. In this content, the designed nanocomposites can generate two types of ROS: superoxide anion radicals ($O_2^{\cdot -}$) and $^1O_2$, achieving multimodal PDT. Moreover, hydrogen therapy has also received considerable attention due to its inherent biosafety. Wang et al. reported a multimodal therapy nanoplatform by combining PDT, PTT, and hydrogen therapy together in which g-C_3N_4 nanosheets doped by Cu_3P and UCNPs NPs were encapsulated by a ZIF-8 shell, followed by post-modifications with folic acid, constructing a hydrogen self-generation system via water splitting under NIR irradiation [114].

2.2.3. IONPs

Given the biocompatibility and availability of IONPs, their remarkable properties have received significant attraction over the last decades that has further led to considerable efforts in fabricating their use for biological applications [79,115–118]. For example, IONPs can be optimized in the construction of therapeutic nanoplatforms for bio-catalysis, bio-imaging, chemotherapy, PDT, and hyperthermia therapy applications. As there is no denying that noble metal-based MOF nanocomposites tend to be relatively more expensive than other nanomaterials, Fe_3O_4 NPs have sparked widespread interest in their cost-effective use as nanozymes since 2007 [119]. One report demonstrated that they displayed similar catalytic properties of horse radish peroxidase (HRP) [120]. Moreover, the combination of functional IONPs with MOFs results in the formation of magnetic framework composites (MFC) [21,51], presenting advantages such as high porosity and reliable magnetic properties for bio-catalytic applications [21,51]. It has also been reported that MIL-88(Fe) and MIL-101(Fe) possess POD-like activity [121]. In this content, Zhang et al. assembled a Fenton-like system using Fe_3O_4 NPs combined with MIL-88 which improved the catalytic efficiency of generating hydroxyl radicals for the selective detection of reduced glutathione [122]. Their strategy was to use the "bottle-around-ship" approach to introduce the MAA-modified Fe_3O_4 into the MOF precursor solution to form MFC. Even though the post-modified Fe_3O_4 was incorporated using this method, it did not form a "bottle-around-ship" structure, but rather a physical mixture of Fe_3O_4 NPs with MOF materials. As such, it should be noted that the selection of MOF materials and appropriate synthetic conditions play a key role in achieving a "bottle-around-ship" structure. Moreover, Wu et al. reported an artificial enzyme, Fe_3O_4@MIL-100(Fe), that was synthesized by growing MIL-100 layer around carboxylic acid-modified Fe_3O_4 NPs core through the "bottle-around-ship" approach [123]. Further, a "layer--by-layer" strategy was used to grow the MOF shells for 20 cycles to increase the pore volume and S_{BET} [56]. This artificial enzyme was found to detect cholesterol as low as 0.8 μM [123]. In one recent study, Bagheri et al. prepared a physical mixture of two pre-synthesized Fe_3O_4 NPs and MOF materials to detect organophosphorus, possessing a detection limit of 0.2 nM for diazinon [124]. Another physical mixture example is reported by Tang et al. in detecting glucose with a limit of 4.9 nM [125]. MFC nanocomposites are not only regarded as nanozymes, but also have the ability to immobilize and encapsulate enzyme [126–128] due to the porosity properties of MOFs [24]. Several studies have demonstrated this unique phenomenon. Zhai et al. reported the encapsulation of Fe_3O_4 NPs into ZIF-90 to immobilize trypsin [129]. Cao et al. encapsulated both cellulose-coated Fe_3O_4 NPs and enzyme into ZIF-8, showing an enhanced catalytic activity compared with free enzymes [130]. However, their work demonstrates that the immobilization methods may have influenced the conformation change of the enzyme, subsequently enhancing enzymatic activity. Furthermore, Ricco et al. encapsulated both Fe_3O_4 NPs and the enzyme into ZIF-8 via one-pot synthesis [131]. The enzymatic activity of this nanocomposite was assessed by the reaction of pyrogallol with hydrogen peroxide, displaying an enzymatic activity that is five times higher compared to that of enzyme-encapsulated ZIF-8 composites. Thus, this study showcased the ability of Fe_3O_4 NPs in enhancing catalytic performance. Alternatively, Lin et al. demonstrated a different strategy in encapsulating both IONPs and enzyme into MOFs by coating the MOF on the outer surface of polydopamine-functionalized Fe_3O_4 NPs to fabricate the MFC nanocomposites and later immobilized with amidase. Through this method, no significant catalytic activity loss was found after storing at 4 °C for five months [132]. In addition, loading Fe_3O_4 NPs with other nanozymes onto the MOF structure can also increase catalytic activity. This strategy has been demonstrated by Tan et al., in which Au and Fe_3O_4 NPs were both loaded onto a MOF nanosheet, achieving a detection limit as low as 1.7 ppb of sulfadimethoxine [133].

As aforementioned, encapsulating IONPs into the structure of MOFs has presented many advantages when utilized as nanozymes for POD- and CAT-mimetic catalytic reactions. Such biological examples include producing ROS or detecting glucose. Furthermore, IONPs can also be used as a magnetic heating mediator by generating heat from the external electromagnetic energy via Néel-Brownian relaxations [134]. When utilized in cancer cell treatments, IONPs create heat shock responses in tumor cells. Subsequently, cell destruction ensues. As such, the properties of IONPs can be tailored in constructing an effective instrument for various biological applications in producing a thermoresponsive feedback, such as the use of magnetothermal triggered cargo delivery. Moreover, several carriers have been used to prepare a core-shell structure with IONPs, such as silica NPs, polymer, and graphene [135]. Likewise, given the porosity and highly crystallized structure of MOFs, this material can also be used as a carrier to load IONPs to achieve magnetothermal triggered cargo delivery. In one early study, Kaskel's group demonstrated the integration of superparamagnetic IONPs in polycrystalline MOF aggregates [136]. Since then, there have been many subsequent studies on IONPs-functionalized MOF nanocomposites [51,137–139]. In this study, the obtained nanomagnet-functionalized MOFs with superparamagnetism can be heated under an AMF, resulting in an increased release rate of ibuprofen. Their remarkable work is one of many early notable studies that promoted the use of MOFs as carriers for IONPs in magnetothermal-triggered drug release applications. Given the surface properties of IONPs, several surface functional groups are used to pretreat the surface of IONPs to increase the opportunities of constructing IONP@MOF nanocomposites. Different surface functional groups will be discussed to classify the various designs of IONP@MOF nanocomposites, along with their cancer therapy application.

Since carbon-coated IONPs (Fe_3O_4@C) present a hydrophilic carboxyl on the surface, this can contribute to the growth of the MOF layer around the IONPs [140]. This method has been reported by many groups in constructing IONP@MOF nanocomposites [141–143]. He et al. [142] have demonstrated the growth of ZIF-8 around Fe_3O_4@C, and further loaded with DOX inside of the framework, displaying pH-responsive chemotherapy *in vivo*. Additionally, Wang et al. have demonstrated the growth of a MIL-100(Fe) layer around Fe_3O_4@C and further loaded with a hydrophobic drug, dihydroartemisinin (DHA). Under acidic conditions, the MIL-100 layer was degraded and released

Fe^{3+}, while DHA would be further released. Subsequently, this resulted in the generation of Fe^{2+} by reducing Fe^{3+} and ultimately reacting with DHA to produce ROS and induce cell death [141] (Fig. 5A). Furthermore, silica-coated IONPs have also been used to design IONP@MOF nanocomposites [144].

As aforementioned, PVP is widely used as a capping agent as well as an amphiphilic, non-ionic polymer agent in assisting the assembly of MOF-based nanocomposites (Fig. 5B). Many groups have reported PVP-functionalized IONPs@MOF for drug delivery, cancer therapy applications [52,53,145–147]. Fang et al. have shown a low frequency AMF-responsive drug delivery nanoplatform by encapsulating PVP-modified Gd_2O_3 and Fe_3O_4 into a ZIF-90 framework via "bottle-around-ship" method [53]. In another study, Yang, and the co-workers [146] designed a multistimuli-responsive therapeutic nanoplatform by growing UiO-66 shells around PVP-modified Fe_3O_4, followed by drug loading and the post-modification with carboxylatopillar[6]arene. Zhou et al. loaded both lactate oxidase and PVP-functionalized Fe_3O_4 into a ZIF-8 framework via a one-pot method. H_2O_2 was generated by the catalytic reaction of lactate and subsequently, converting to hydroxyl radicals which is further catalyzed by Fe_3O_4, inducing tumor cell death [145]. TEM, powder-XRD (PXRD), and dark-field imaging confirmed the encapsulation of Fe_3O_4 into the ZIF frameworks with the corresponding elemental mappings (Fig. 5C).

Moreover, carboxylic acid ligands can be also used to decorate IONPs, assisting the assembly of MOFs through various growth mechanisms [57,137] (Fig. 5D). Zhao et al. designed a poly (acrylic acid)-functionalized Fe_3O_4@UiO-66 nanocomposite via *in-situ* growth with a high transverse relaxivity, demonstrating their potential utility to serve as a T_2 contrast agent [148] (Fig. 5E). Further, DOX was loaded into the nanocomposites with 2.0 mg DOX per mg of nanocomposites. Additionally, MAA can also be used to decorate Fe_3O_4 to aid in the assembly of Fe_3O_4@MOF nanocomposites. Wang et al. prepared a heterojunction structure by conjugating MAA-functionalized Fe_3O_4@MIL-100(Fe) with polyethyleneimine-coated UCNPs, ultimately displaying hypoxia tumor therapy effects [58]. Moreover, Chen et al. reported the use of polydopamine to modify Fe_3O_4 in fabricating nanocomposites [54]. Remarkably, the constructed nanocomposites display synergistic magnetic hyperthermia and chemotherapy.

2.2.4. $MnFe_2O_4$ NPs

Mixed ferrites (MFe_2O_4 where M = Zn, Co, Ni or Mn) can be synthesized by doping IONPs with other additional metallic elements, and notably, enhance the catalytic activity of IONPs [149]. Zhang et al. designed a $MnFe_2O_4$@MOF core-shell nanocomposite by growing porphyrin-based MOF shells around $MnFe_2O_4$ NPs, showing both glutathione (GSH) POD-like and CAT-like activities. $MnFe_2O_4$ NPs in this

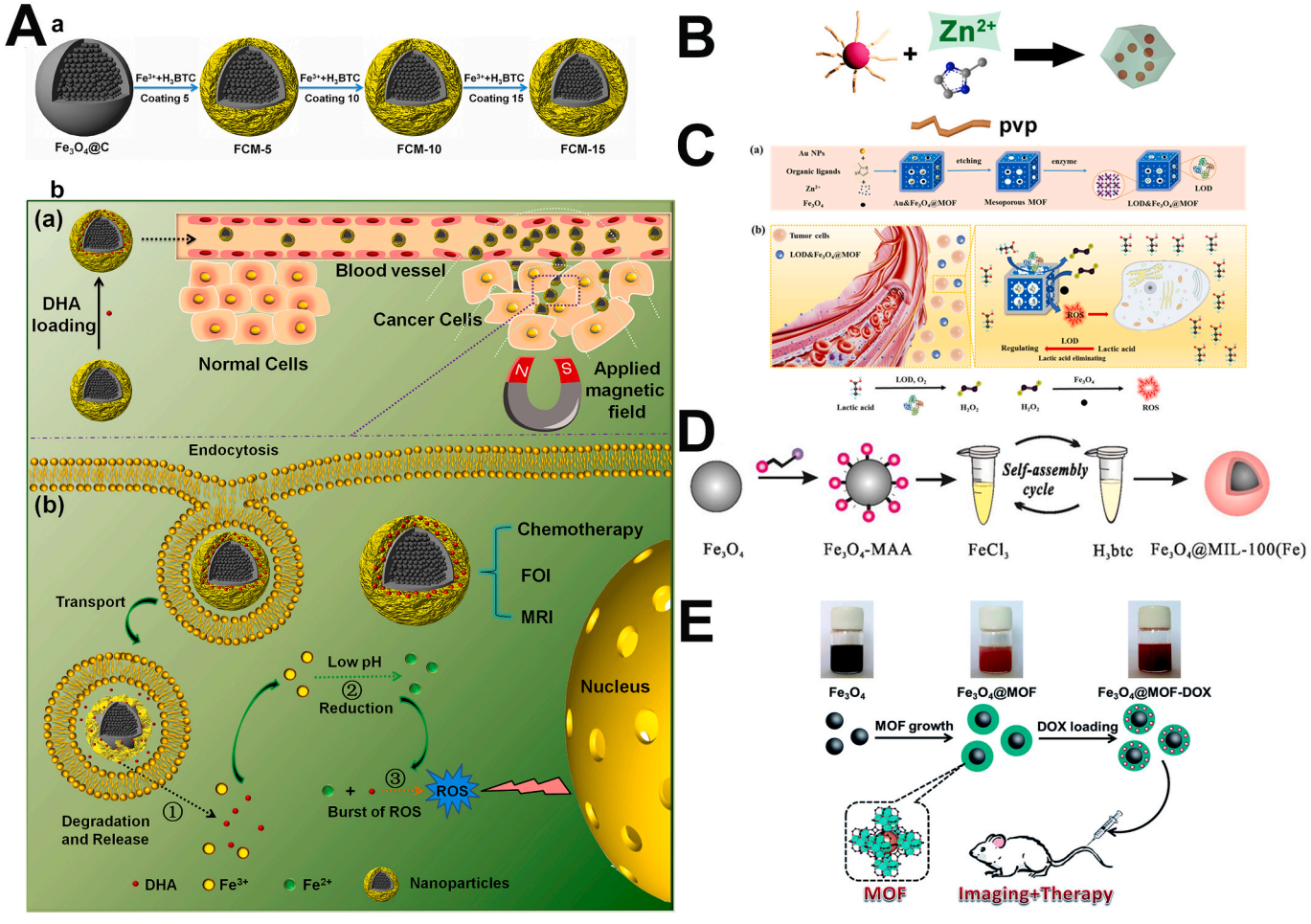

Fig. 5. (A) (a) A schematic illustration for the synthesis of Fe_3O_4@C@MIL-100(Fe) (FCM) therapeutic NPs; (b) Schematic illustration of targeting of DHA loaded FCM nanoparticle to tumor cells assisted by an externally applied magnetic field (a) and the anticancer mechanism of the DHA delivery system [141]. Reproduced with permission. Copyright 2016, *Biomaterials*. (B) Schematic illustration for fabrication process of PVP-modified IONPs with ZIFs. (C) (a) Illustration of the synthesis of lactate oxidase & Fe_3O_4@ZIF-8 NPs. (b) Tandem biological–chemical catalytic reactions for effective catalytic tumor treatment based on the characteristic of the TME [145]. Reproduced with permission. Copyright 2020, *ACS Appl. Mater. Interfaces.* (D) Schematic illustration of the synthetic procedure for the preparation of Fe_3O_4@MIL-100 [57]. Reproduced with permission. Copyright 2015, *ACS Appl. Mater. Interfaces.* (E) Schematic of the fabrication of Fe_3O_4@MOF core–shell composites for imaging and therapy [148]. Reproduced with permission. Copyright 2016, *Chem. Sci.*

nanocomposite could catalyze endogenous H_2O_2 to generate O_2. It is widely known that GSH, a free radical scavenger, could neutralize the ROS produced under light exposure, thus decreasing the efficiency of PDT. In this content, the constructed nanocomposites could use the produced oxygen to consume GSH with laser exposure, achieving enhanced PDT efficacy. As compared with pure MOF, $MnFe_2O_4$@MOF shows a reduction of 71% in GSH content after incubation for 3 h. The T_1 and T_2 relaxation rate for $MnFe_2O_4$@MOF were 2.94 and 51.53 mg^{-1} mL s^{-1} which showed promising potential for imaging-guided cancer therapy [150] (Fig. 6A).

2.2.5. MnO_2 NPs

MnO_2 with CAT-like activity can also be used as an O_2 producer by sustainably catalyzing the endogenous H_2O_2. As H_2O_2 is frequently overexpressed in a tumor microenvironment, the post-generated O_2 effectively alleviates tumor hypoxia, significantly improving PDT and chemotherapy effects [151]. Zhang et al. designed an all-in-one ZIF-8--based nanocomposites by loading MnO_2 nanodots into the framework and surface-modifying F127 outside of the framework. The DOX and g-C_3N_4 were co-encapsulated into the ZIF-8 frameworks via a one-pot approach. Furthermore, under visible light exposure (660 nm), g-C_3N_4 can generate ROS with oxygen produced by the MnO_2-catalysis reaction of H_2O_2, ultimately showing enhanced PDT effects [152].

2.2.6. CuS

CuS NPs, are among the most commonly utilized PTT reagents in constructing chemo-PTT nanocomposites. For example, one study reported the encapsulation of CuS NPs into ZIF-8, followed by DOX loading into the nanocomposites, showing both chemo and photothermal therapeutic effects [153]. Moreover, Jiang et al. [154] used the "bottle-around-ship" approach to grow a ZIF framework around the pre-synthesized CuS NPs, constructing CuS@ZIF-8 nanocomposites. Further, the nanocomposites were loaded with quercetin and surface-modified with a targeting agent, folic acid-bovine serum albumin. This chemo-photothermal therapeutic nanoplatform demonstrated NIR-triggered and pH-responsive release behaviors, showing superior anticancer effects over the chem- or phototherapy alone both *in vivo* and *in vitro*.

2.2.7. Cerium oxide NPs

Ceria has long been used as an antioxidant to treat illnesses of the central nervous system such as Alzheimer's disease [155]. Because of the electron transfer between cerium(III) and cerium(IV), cerium is also recognized as a nanozyme with characteristics of ROS scavenging activity. In one study, Yu et al. constructed a nanozyme, CeNPs@MIL-100, by growing MIL-100 around PVP-coated CeO_2 NPs. The retinoic acid (RA) and small interfering RNA (siSOX9) were co-loaded into the CeNPs@MIL-101 carriers. Due to the antioxidative properties of ceria, the newborn neurons can thereby be protected from oxidative damage. Additionally, the released siSOX9 and RA from the MOF carriers have the ability to cooperate together to control the differentiation of neural stem cells to neurons, resulting in fewer neuronal apoptosis and enhanced cognition impairment in Alzheimer's disease [156] (Fig. 6B). Liu et al. [157] also reported a cerium oxide NPs@MIL nanocomposite for enhanced PDT. Due to amino group existing on the MOF ligands, the nanocomposites can be post-modified with poly(ethylene glycol)-folate and cyanine 3-labelled caspase-3 substrate peptide, exhibiting a target delivery and response to caspase-3.

2.2.8. Quantum dots (QD)

Lei's group [33] constructed a sandwich-like structure QD/MOF/-MOF, via a "bottle-around-ship" approach by growing the MIL shells around PVP-functionalized black phosphorus QD, followed by encapsulating another MIL-stabilized CAT layer outside of QD@MOF nanocomposites. The outer layer of the sandwich-like structure can be regarded as a tandem catalyst to generate oxygen by catalyzing H_2O_2. Further, the injected oxygen was photocatalyzed by black phosphorus QDs in the inner core, resulting in a high quantum production of $^1O_2$.

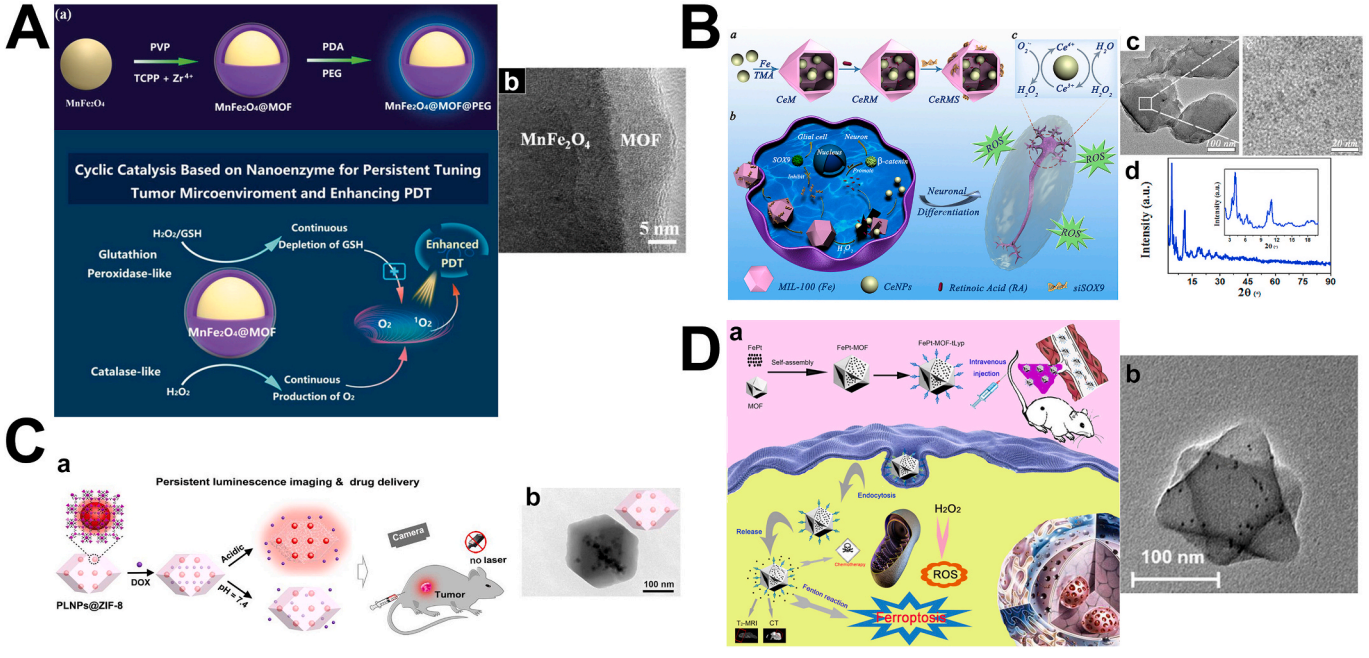

Fig. 6. (A) Schematic illustration of the synthetic process of core–shell nanostructure and $MnFe_2O_4$@MOF for persistently providing O_2 and consuming GSH to efficiently enhance PDT; (b) HRTEM of $MnFe_2O_4$@MOF [150]. Reproduced with permission. Copyright 2019, *Adv. Funct. Mater.* (B) (a) Preparation process of CeNPs/RA@MIL-100/siSOX9 (CeRMS); (b) Schematic illustration of neuron-directional differentiation and neuroprotection for enhanced neurogenesis; (c) TEM image of CeNPs@MIL-100 (CeM) and its magnification; (d) PXRD patterns of CeM [156]. Reproduced with permission. Copyright 2020, *Biomaterials.* (C) (a) Schematic illustration of persistent luminescence imaging and drug delivery; (b) TEM image of as-prepared PLNPs@ZIF-8 [159]. Reproduced with permission. Copyright 2019, *Biomaterials.* (D) (a) Fabrication process of FePt-MOFs-tLyp-1 NCs and the mechanism of pH-Responsive Bionanocomposites for ferroptosis therapy and MRI/CT Imaging; (b) TEM images of FePt(R)-MOF nanocomposites [161]. Reproduced with permission. Copyright 2020, *ACS Appl. Nano Mater.*

The apoptotic percentage of hypoxic cell was 52.1%, which is 8.7-fold compared with QD@MOF@MOF nanocomposites without CAT stabilization.

2.2.9. Persistent luminescent NPs (PLNPs)

Persistent luminescence is a phenomenon of long-lasting luminescence for hours or days without continuous external irradiation, which is significant for background interference-free sensing and bio-imaging. Lv et al. [158] and Zhao et al. [159] used the one-pot strategy to encapsulate PLNPs within ZIF-8 frameworks. Further, DOX was loaded inside of the nanocomposites. The DOX-loaded PLNP@ZIF-8 nanocomposites exhibited persistent luminescence tumor imaging both *in vivo* and *in vitro* under an acidic environment (Fig. 6C). Followed by this work, Chen et al. used the "bottle-around-ship" approach to grow MOF shells around the carboxylic acid-modified PLNPs. After pyrolysis of the obtained nanocomposites (PLMC), the pore size increased, further accommodating for the use of three model drugs. After coating the macrophage membrane onto PLMC, the final nanoplatform was found to be capable of tumor therapy and permanent luminescence imaging-guided drug delivery with fluorescence-free background [160].

2.2.10. FePt

In a tumor microenvironment, FePt NPs with face-centered cubic systems release Fe in the tumor microenvironment catalyzing H_2O_2 to produce oxygen and induce ferroptosis. With this regard, ROS can be generated by converting oxygen to induce cell death. Due to the superparamagnetic properties, FePt NPs can also be used for computed tomography (CT) and magnetic resonance (MRI) imaging. Meng et al. designed FePt-MOF nanocomposites by loading FePt NPs, whose diameter is 1–2 nm, into iron-based MOF, showing cell eradication and tumor imaging [161] (Fig. 6D). Table 1 summarizes other nanoparticle-based metal-organic framework nanocomposites for biomedical applications since the synthetic methods for those nanocomposites are hard to classify into general methods.

3. MOF-integrated nanoplatforms

3.1. SiO_2 platform

Silica nanoplatforms have received significant attention for biomedical applications as they possess a variety of nanoscale properties such as porosity, stability, and hydrophilicity. Moreover, Silica NPs can help promote the growth of MOF NPs. Ke et al. prepared porous Fe-based MOF nanocomposites using a MIL-100(Fe) core with a silica shell as carriers for immobilizing gallic acid (GA). Their findings reveal that MIL-100(Fe)@SiO_2 significantly enhances GA's antioxidant activity while in a PBS solution [181].

3.2. Graphite oxide (GO) nanosheets

Graphene oxide possesses properties of easy functionalization and strong hydrophilicity, suitable for the dispersion of MOF NPs. The presence of oxygen-rich functional groups, hydroxyl and carboxylic groups allow the possibility of GO to grow other NPs on their surface. Wang et al. used graphene nanosheets to bind to polydopamine (PDA)/ZIF-8 microcapsules through π-π stacking and hydrogen bonding, achieving superior electrochemical activity and conductivity. Further, GOx was loaded into the (PDA)/ZIF-8@graphene microcapsule and a glassy carbon electrode was used to immobilize the capsule to form a sensing platform, displaying a detected concentration of glucose as low as 0.333 μM [182]. Meng et al. [183] prepared MOF/GO nanosheet composites through condensation reactions to link amine-functionalized MOF with carboxylic acid-functionalized GO nanosheets, achieving PTT effects. Zhu et al. designed a ZIF-8/GO nanocomposites by growing ZIF-8 on the external surface of GO for cytochrome *c* (Cyt *c*) encapsulation. This study showed that the ZIF-8/GO nanocomposites had the

Table 1
Other nanoparticle-based metal-organic framework nanocomposites for biomedical applications.

Nanoparticles	MOFs	Additional functional groups or materials	Drug or enzyme	Applications	Ref
Magnetic carbon NPs	MIL-100	4,4′-diamino-2,2′-bipyridine (DABPY) and Mn $(CO)_5Br$	DOX	Carbon monoxide therapy, Chemotherapy, PTT	[162]
ZnS	ZIF-8		Indocyanine green (ICG) and tirapazamine	H_2S-amplified synergistic therapy	[163]
PPy NPs	MIL-100	PVP	DOX	PTT and chemotherapy	[164]
Graphene QD NPs	ZIF-8		DOX	PTT and chemotherapy	[165]
g-C_3N_4 nanosheets	ZIF-8		DOX	PDT and chemotherapy	[166]
$NaLnF_4$	Ln-based MOF	PVP	DOX	Drug delivery and cell imaging	[167]
Maghemite NPs	MIL-100 (Fe)	Citrate	DOX	T_2-magnetic resonance imaging and drug delivery	[168]
Fe_3O_4	UiO-66-NH_2	Polyacrylic acid and graphdiyne	DOX	Chemotherapy	[169]
UCNPs	MIL-100	PEG (polyethylene glycol)	DOX	Drug delivery and luminescence/magnetic resonance imaging	[170]
Au NPs	ZIF-8, Eu_x, Tb_y	PVP	5-FU	Drug delivery	[171]
UCNPs	ZIF-8	5,10,15,20-tetrakis(4-aminophenyl)porphyrin (TAPP) and glutaraldehyde	CAT and glucose oxidase	PDT and starvation therapy	[172]
Fe-DOX NPs	Gd-MOF	PVP and poly-(sodium 4-styrenesulfonate)	ICG	PDT and chemotherapy Multimodal imaging	[173]
Se or Ru NPs	MIL-101		Small interfering RNAs (siRNA)	Multidrug Resistance in Taxol-resistant breast cancer cells	[174]
UCNP	UiO-66-NH_2	Folic acid	DOX	Imaging and chemotherapy	[175]
Fe_3O_4	Bio-MOF	Folic acid and chitosan	5-FU	T_2-imaging and chemotherapy	[176]
Fe_3O_4	IRMOF-3	*O*-carboxymethyl chitosan and carbon dots	DOX	Target anticancer drug delivery	[177]
Au nanocage and Fe_3O_4	MIL-101-NH_2	polydopamine	DOX	PTT and chemo therapy	[178]
$NaGdF_4$:Yb/Er	MIL-53(Fe)	Folic acid	DOX	Tumor-targeting chemotherapeutic delivery	[179]
UCNPs	MIL-53-NH_2	PVP, folic acid and PEG	DOX	Drug delivery	[180]

ability to prevent protein leakage and preserve the activity of the enzyme under ethanol and acetone storage compared with ZIF-8 and GO themselves. Furthermore, the Cyt *c*-loaded ZIF-8/GO nanocomposites did not lose enzymatic activity after four cycles [184].

3.3. Metal polyphenol networks (MPNs)

MPNs are supramolecular network materials assembled by metal ions and phenolic ligands; they can be utilized as coating materials on the various substrates like MOFs and silica nanoparticles [185], due to their high affinity with the substrates. Tannic acid (TA) as a phenolic ligand is commonly used to create MPNs with antibacterial, antioxidant and anticarcinogenic properties [186]. Zhang et al. [187] designed a Fenton nano system regulated by adenosine triphosphate (ATP), called GOx@ZIF@MPN, in which the nanocomposite was coated outside with a MPN via one-pot approach. Due to the overexpression of ATP in tumor cells, degradation of the outer MPN shell resulted in Fe(III) and TA. Moreover, Fe(III) can be reduced by TA to Fe(II). Further, this disassembled ZIF structure led to the exposure of GOx, resulting in the production of H_2O_2 by endogenous glucose which is catalyzed by Fe(II) to produce toxic hydroxyl radicals. As a result, starvation therapy and enhanced chemo dynamic therapy were demonstrated as this Fenton nano system exhibited tumor ablation in 4T-1 tumor-bearing mice.

4. MOF-derived nanocomposites

Recently, MOFs have been recognized as potential sacrificial templates for constructing different mesoporous carbon nanostructures with robust stability and high conductivity via high-temperature pyrolysis [188,189]. By controlling the temperature and time of pyrolysis, the metal oxide or metal nanostructure with different shapes like hollow, sheets and rods, etc., could also be afforded. Compared with the parent MOFs, MOF derivatives preserve the porosities and periodic crystalline structures, thus rendering a confined space for metal species and other heteroatoms [190]. Moreover, MOF-derived carbon structures offer higher chemical stability and can overcome the drawbacks of the parent MOFs thereby broadening their practical application scope [191]. Herein, we will only summarize the nanocomposites derived by MOF pyrolysis, not the single atom within the framework [192].

4.1. ZIF-derived nanocomposites

Through the coordination of imidazolates and tetrahedral metal ions, ZIFs possess high chemical and thermal stabilities. Interestingly, dodecahedral ZIF-67 is widely derived to construct the hollow nanostructure [190], thus providing high loading capacity for active nanoparticles. Zhao et al. loaded Fe NPs into ZIF-67-derived Co_3O_4 hollow nanocages, exhibiting superior POD-like activity compared with pristine Fe NPs and Co_3O_4 hollow nanocages alone. This nanocomposite can be used to detect glucose with the limit of 0.05 μM [193]. With the high content of nitrogen and large surface area, ZIF-8-derived carbon materials offer extra binding sites for loading additional functional particles. Mou et al. prepared a nanozyme cascade bio-platform, BSA-PtAu@CNS, by doping bovine serum albumin (BSA)-coated Pt and Au NPs on the carbon nanosheet derived from ZIF-8. The nanozyme bio-platform obtained a linear range from 2 μM to 2 mM for H_2O_2 and the K_m for H_2O_2 was found to be 0.005 mM [194].

Notably, by doping the transition metal into ZIFs-derived carbon structures, these nitrogen-containing precursors have a similar metal coordination center compared with the porphyrin macrocycle. In addition, the incorporation of mesoporous silica outside of ZIF materials as a coating shell can prevent the agglomeration of nanoparticles under high-temperature pyrolysis conditions [192]. Liu's group [195,196] proposed a new strategy to create porphyrin-like zinc center (PMCS) by surface coating mesoporous silica around ZIF-8 nanoparticles, followed by high-temperature pyrolysis and finally removal of mesoporous silica shells through etching. The PMCS could avoid the problem caused by the conventional porphyrin macrocycle such as instability, poor penetration depth and low activity of photosensitizer. Surprisingly, the photothermal conversion efficiency of PMCS obtained was 33% compared with other widely used photothermal agents. The efficiency for generating $^1O_2$ was increased by 203.6% under ultrasound. The PMCS displayed a tumor inhibition efficiency of 85%. This revealed that MOF-derived mesoporous carbon could play an important role in future cancer therapy applications. Further, they used a ZIF template to build a double-layer hollow silicate nanoparticles with doping manganese (DHMS) for multimodal imaging-guided sonodynamic therapy [197] (Fig. 7A).

Bimetallic ZIFs-derived N, Co-doped porous carbons have some notable advantages in comparison with the individual ZIF component [73], including higher porosity, graphitization degree, stability and electrical conductivity. Wang et al. designed a "three-in-one" therapeutic nanoplatform, CuCo(O)@PCNs, through pyrolysis and calcination of Cu-doped ZIF-8@ZIF-67. Further, DOX was loaded into the nanoplatform achieving PTT, starvation and immunotherapy. The photothermal conversion efficiency of CuCo(O)@PCNs was 40.04%, providing evidence that this system can be used to ablate the primary tumor. Furthermore, CuCO(O), a nanozyme, can be used to consume GOx to achieve starvation therapy [198] (Fig. 7B).

4.2. MIL-derived nanocomposites

Magnetic porous carbons derived from iron-based MOFs possess the advantage of preventing the aggregation of the spatially confining nanoparticles. Dong et al. embedded Co NPs into MIL-derived carbons with magnetic and porous properties. This nanocomposite has a strong POD-like activity compared with the pure Co NPs and magnetic carbons, reaching a detection concentration of glucose as low as 156 nM [199].

Fe_3O_4 derived from iron-based MOFs improved the microwave absorption and reduced the electromagnetic loss, and thus can facilitate the energy transfer from electromagnetic energy to heat [200]. Such characteristics present clinical therapeutic opportunities for its prospective utility as an efficient magnetic hyperthermia agent. Xiang et al. prepared a DOX-loaded Fe-MOF-derived porous Fe_3O_4@C nanocomposites, attaining a combined cancer therapy with chemotherapy and hyperthermia effect. When the nanocomposites were irradiated by an AMF (898 kHz and 4.8 kA m^{-1}), the solution temperature was found to increase to over 60 °C. Subsequently, this high temperature caused a hyperthermia effect, promoting the release of DOX, and thus inducing cancer cell death [201].

5. Conclusion and challenges

In this review, we discussed the recent advances in developing MOF-based nanocomposites for biomedical applications and classified these nanomaterials by various NPs integrations to help guide future studies in understanding the different approaches in design and formulation strategies. As the "bottle-around-ship" and "one-pot" methods were the most commonly utilized approaches for constructing MOF nanocomposites, we believe that our review will help contribute to the progression of exploring more versatile strategies to fabricate MOF-based nanocomposites. Further, it is our hope that this review will help advance the use of multimodal therapeutic nanoplatforms for enhanced cancer therapies across medical disciplines. For example, recently, Chen group and our group systematically evaluated a series of pure MOFs for cosmetic and cutaneous applications [202]. These multifunctional MOFs laid a foundation for establishing MOF-based nanocomposites with multimodal therapeutic effect.

Despite the significant potential of MOF-based nanocomposites as promising solutions for the biocatalytic and cancer therapy field, several limitations remain to be addressed: (1) The most frequently used approach to construct MOF-based nanocomposites, the "bottle-around-

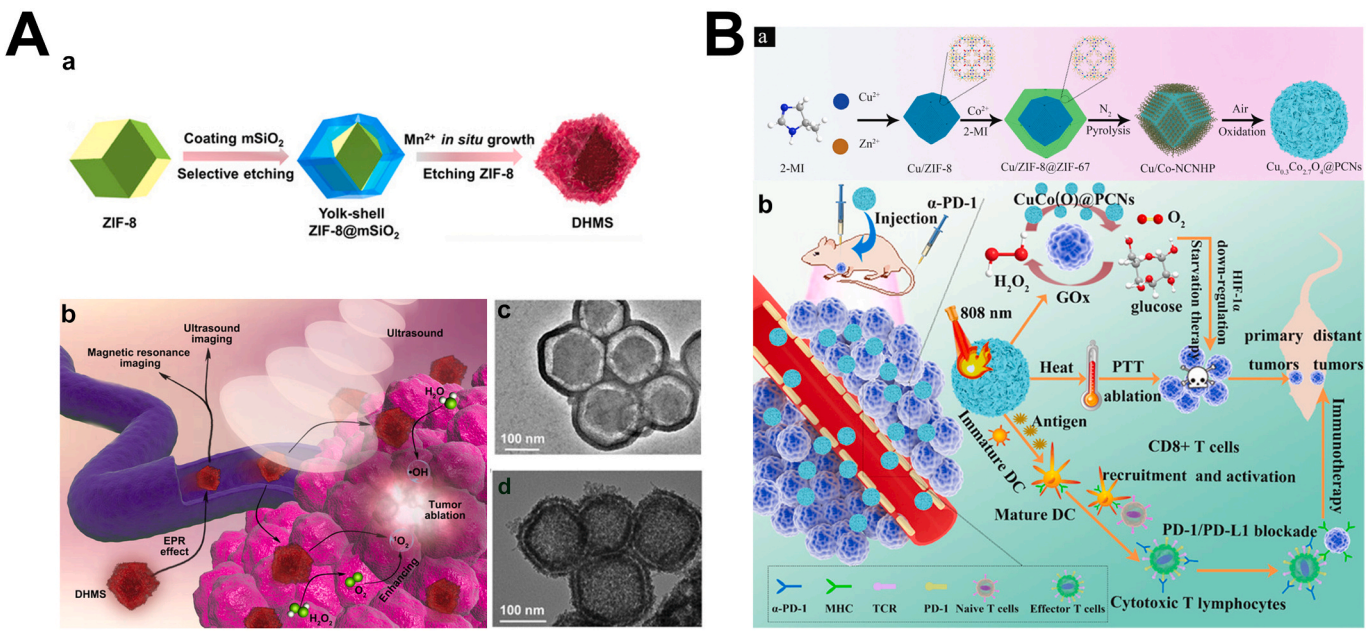

Fig. 7. (A) (a) Scheme of the synthesis process for DHMS; (b) Schematic illustration of DHMS for multimodal imaging guided sonodynamic therapy; TEM images of (c) yolk–shell ZIF-8@mSiO$_2$ and (d) DHMS [197]. Reproduced with permission. Copyright 2020, *Angew. Chem., Int. Ed.* (B) (a) Fabrication procedure of the CuCo(O)@PCNs nanoenzyme; (b) Schematic illustration of the ZIFs-derived nanozyme CuCo(O)@PCNs with three-in-one functions to achieve synergetic therapy [198]. Reproduced with permission. Copyright 2021, *ACS Appl. Mater. Interfaces.*

ship" method, involves integrating pre-synthesized NPs into the MOF precursor solution in order to assemble the MOF structure around the NPs; subsequently, the resulting nanocomposites preserves the shape of the pristine NPs, leading to low porosity and small surface area, thus low drug loading amount. (2) Although surface functional groups may assist in assembling MOFs by modifying NPs via ligand exchange methods, the construction of NPs@MOF nanocomposites still remains challenging due to the susceptibility of nanoparticle self-aggregation, which arises from their low exchange ratio and the reversible ligand exchange process; in this content, PXRD analysis alone is inadequate to verify the presence of nanocomposites, which can be overcome by using large scale TEM and SEM images. (3) The absence of PXRD characteristic peaks of MOFs after encapsulating the functional materials into MOFs indicates the transformation into an amorphous phase for the nanocomposites, which could restrict their employment for application in biological disciplines. (4) In comparison with the parent MOFs and/or the functional materials, enhanced and/or synergistic properties are anticipated with the development of MOF-based nanocomposites, although most studies did not demonstrate such characteristics. For example, nanocomposites constructed by porphyrin-based MOFs and upconversion nanoparticles have been used to produce singlet oxygen for PDT application. It is needed to discuss whether the construction of such nanocomposites is rational if there is a lack of enhanced therapeutic effects. Moreover, Au nanoparticles are regarded as PTT agents as well as biomimetic enzymes. For the construction of MOF-based nanocomposites with Au nanoparticles, future research should explore their synergistic effect compared with a simple physical mixture of two materials. (5) Although some MOF-based nanocomposites have been extensively explored *in vitro* and *in vivo*, more studies should investigate if the therapeutic effect arise from the nanocomposites or the individual components. (6) There are a limited number of studies that demonstrate whether the NPs are integrated inside or outside of the nanocomposite structures; further elucidation of this context can help to enhance our understanding of the combined or synergistic properties of MOFs and NPs in nanocomposites, especially for biological systems. (7) Many MOF-based nanocomposite studies assess the efficacy of DOX for its chemotherapeutic effects, however, the size of this drug is 1.5 × 1.0 × 0.7 nm [160], which is larger than some MOF pores, such as ZIFs and UiO-66s; should studies explore the efficacy of this drug loaded on MOF carriers, researchers need to demonstrate whether DOX can be effectively loaded inside or attached outside of the MOF structure. (8) Future studies must also consider the safety limit for human exposure when employing laser and magnetic field instruments. For example, the safety parameter for the product of frequency and magnetic field amplitude was suggested to be less than 5×10^9 Am^{-1}s^{-1} [203]. Moreover, improvements in the tissue penetration can be made by appropriately selecting emission and excitation bands of laser within "optical windows". (9) By catalyzing intracellular H_2O_2 in tumor cells, the use of nanozymes as an O_2 supplier such as MnO_2, Au, FePt and $MnFe_2O_4$ nanoparticles, are widely employed for the construction of MOF-based nanocomposites in an effort to relieve the tumor hypoxia. Many studies claim that the porous feature of MOFs can improve the diffusion of O_2 and $^1O_2$, and thereby enhance PDT efficacy. However, as mentioned in limitation (1), most nanocomposites inherit the shape of nanoparticles. As such, it is necessary to address the functionality of MOF shells in nanocomposites. Moreover, future research should explore and determine which nanozymes are the most effective for constructing MOF-based nanocomposites. This is also often overlooked in PTT application with MOF-based nanocomposites assembled with graphene, CuS, and Au nanoparticles. Furthermore, it is unnecessary to encapsulate different nanoparticles into MOF structures for the same biomedical application without determining their synergistic enhancement effects. This is a crucial finding that can help guide future studies in developing more advanced biomedical nanocomposites.

In summary, early reports of MOF-based nanocomposites have shown encouraging results for biomedical applications. While these nanomaterials display remarkable potential, there are some challenges warranting the consideration and further exploration in future research. With increasing attention to the recent development of MOF-based nanocomposites, the utilization of these nanocomposites offers exciting new avenues for the clinical advancement of nanotechnology in biomedicine.

Declaration of competing interest

The authors declare that they have no known competing financial interests or personal relationships that could have appeared to influence the work reported in this paper.

Acknowledgement

The authors acknowledge NSF (DMR-1352065) and the Robert A. Welch Foundation (B-0027) for financial support of this work.

References

[1] H. Jiang, D. Alezi, M. Eddaoudi, A reticular chemistry guide for the design of periodic solids, Nat. Rev. Mater. 6 (6) (2021) 466–487.
[2] R. Freund, S. Canossa, S.M. Cohen, W. Yan, H. Deng, V. Guillerm, M. Eddaoudi, D. G. Madden, D. Fairen-Jimenez, H. Lyu, L.K. Macreadie, Z. Ji, Y. Zhang, B. Wang, F. Haase, C. Woll, O. Zaremba, J. Andreo, S. Wuttke, C.S. Diercks, 25 Years of reticular chemistry, Angew. Chem. Int. Ed. 60 (2021) 23946–23974.
[3] J. Della Rocca, D. Liu, W. Lin, Nanoscale metal-organic frameworks for biomedical imaging and drug delivery, Acc. Chem. Res. 44 (10) (2011) 957–968.
[4] M. Lismont, L. Dreesen, S. Wuttke, Metal-organic framework nanoparticles in photodynamic therapy: current status and perspectives, Adv. Funct. Mater. 27 (14) (2017) 1606314.
[5] P. Gao, Y. Chen, W. Pan, N. Li, Z. Liu, B. Tang, Antitumor agents based on metal-organic frameworks, Angew. Chem. Int. Ed. 60 (2021) 16763–16776.
[6] Y.Z. Chen, R. Zhang, L. Jiao, H.L. Jiang, Metal–organic framework-derived porous materials for catalysis, Coord. Chem. Rev. 362 (2018) 1–23.
[7] K. Lu, T. Aung, N. Guo, R. Weichselbaum, W. Lin, Nanoscale metal-organic frameworks for therapeutic, imaging, and sensing applications, Adv. Mater. 30 (37) (2018) 1707634.
[8] J. Yang, Y.W. Yang, Metal-organic frameworks for biomedical applications, Small 16 (10) (2020) 1906846.
[9] W.-Y. Gao, M. Chrzanowski, S. Ma, Metal-metalloporphyrin frameworks: a resurging class of functional materials, Chem. Soc. Rev. 43 (16) (2014) 5841–5866.
[10] Z. Wang, S.M. Cohen, Postsynthetic modification of metal-organic frameworks, Chem. Soc. Rev. 38 (5) (2009) 1315–1329.
[11] K.K. Tanabe, S.M. Cohen, Postsynthetic modification of metal-organic frameworks-a progress report, Chem. Soc. Rev. 40 (2) (2011) 498–519.
[12] P. Deria, J.E. Mondloch, O. Karagiaridi, W. Bury, J.T. Hupp, O.K. Farha, Beyond post-synthesis modification: evolution of metal-organic frameworks via building block replacement, Chem. Soc. Rev. 43 (16) (2014) 5896–5912.
[13] M. Peller, K. Boll, A. Zimpel, S. Wuttke, Metal-organic framework nanoparticles for magnetic resonance imaging, Inorg. Chem. Front. 5 (8) (2018) 1760–1779.
[14] L. Zhang, Y. Zhou, S. Han, The role of metal-organic frameworks in electronic sensors, Angew. Chem. Int. Ed. 60 (28) (2021) 15192–15212.
[15] S.M.J. Rogge, A. Bavykina, J. Hajek, H. Garcia, A.I. Olivos-Suarez, A. Sepulveda-Escribano, A. Vimont, G. Clet, P. Bazin, F. Kapteijn, M. Daturi, E.V. Ramos-Fernandez, I.X.F.X. Llabres, V. Van Speybroeck, J. Gascon, Metal-organic and covalent organic frameworks as single-site catalysts, Chem. Soc. Rev. 46 (11) (2017) 3134–3184.
[16] R. Medishetty, J.K. Zareba, D. Mayer, M. Samoc, R.A. Fischer, Nonlinear optical properties, upconversion and lasing in metal-organic frameworks, Chem. Soc. Rev. 46 (16) (2017) 4976–5004.
[17] S.A. Younis, N. Bhardwaj, S.K. Bhardwaj, K.H. Kim, A. Deep, Rare earth metal–organic frameworks (RE-MOFs): synthesis, properties, and biomedical applications, Coord. Chem. Rev. 429 (2021) 213620.
[18] W. Zhang, J. Dynes, Y. Hu, P. Jiang, S. Ma, Porous metal-metalloporphyrin gel as catalytic binding pocket for highly efficient synergistic catalysis, Nat. Commun. 10 (1) (2019) 1913.
[19] J. Ren, Z. Niu, Y. Ye, C. Tsai, S. Liu, Q. Liu, X. Huang, A. Nafady, S. Ma, Second-sphere interaction promoted "Turn-on" fluorescence for selective sensing of organic amines in a Tb(III)-based macrocyclic framework, Angew. Chem. Int. Ed. 60 (2021) 23705–23712.
[20] S. Li, F. Huo, Metal-organic framework composites: from fundamentals to applications, Nanoscale 7 (17) (2015) 7482–7501.
[21] P. Falcaro, R. Ricco, A. Yazdi, I. Imaz, S. Furukawa, D. Maspoch, R. Ameloot, J. D. Evans, C.J. Doonan, Application of metal and metal oxide nanoparticles@ MOFs, Coord. Chem. Rev. 307 (2016) 237–254.
[22] Y. Liu, Z. Liu, D. Huang, M. Cheng, G. Zeng, C. Lai, C. Zhang, C. Zhou, W. Wang, D. Jiang, H. Wang, B. Shao, Metal or metal-containing nanoparticle@MOF nanocomposites as a promising type of photocatalyst, Coord. Chem. Rev. 388 (2019) 63–78.
[23] M.d.J. Velásquez-Hernández, M. Linares-Moreau, E. Astria, F. Carraro, M. Z. Alyami, N.M. Khashab, C.J. Sumby, C.J. Doonan, P. Falcaro, Towards applications of bioentities@MOFs in biomedicine, Coord. Chem. Rev. 429 (2021) 213651.
[24] W. Liang, P. Wied, F. Carraro, C.J. Sumby, B. Nidetzky, C.K. Tsung, P. Falcaro, C. J. Doonan, Metal–organic framework-based enzyme biocomposites, Chem. Rev. 121 (3) (2021) 1077–1129.
[25] D. Giliopoulos, A. Zamboulis, D. Giannakoudakis, D. Bikiaris, K. Triantafyllidis, Polymer/metal organic framework (MOF) nanocomposites for biomedical applications, Molecules 25 (1) (2020) 185.
[26] X. Zheng, L. Wang, Q. Pei, S. He, S. Liu, Z. Xie, Metal–organic Framework@ Porous organic polymer nanocomposite for photodynamic therapy, Chem. Mater. 29 (5) (2017) 2374–2381.
[27] J. Liu, J. Huang, L. Zhang, J. Lei, Multifunctional metal-organic framework heterostructures for enhanced cancer therapy, Chem. Soc. Rev. 50 (2) (2021) 1188–1218.
[28] S. Wang, C.M. McGuirk, A. d'Aquino, J.A. Mason, C.A. Mirkin, Metal-organic framework nanoparticles, Adv. Mater. 30 (37) (2018) 1800202.
[29] H.S. Wang, Metal–organic frameworks for biosensing and bioimaging applications, Coord. Chem. Rev. 349 (2017) 139–155.
[30] L.W. Chen, Y.C. Hao, Y. Guo, Q. Zhang, J. Li, W.Y. Gao, L. Ren, X. Su, L. Hu, N. Zhang, S. Li, X. Feng, L. Gu, Y.W. Zhang, A.X. Yin, B. Wang, Metal-organic framework membranes encapsulating gold nanoparticles for direct plasmonic photocatalytic nitrogen fixation, J. Am. Chem. Soc. 143 (15) (2021) 5727–5736.
[31] H. Shen, J. Liu, J. Lei, H. Ju, A core-shell nanoparticle-peptide@metal-organic framework as pH and enzyme dual-recognition switch for stepwise-responsive imaging in living cells, Chem. Commun. 54 (66) (2018) 9155–9158.
[32] S. Sene, M.T. Marcos-Almaraz, N. Menguy, J. Scola, J. Volatron, R. Rouland, J.-M. Grenèche, S. Miraux, C. Menet, N. Guillou, F. Gazeau, C. Serre, P. Horcajada, N. Steunou, Maghemite-nanoMIL-100(Fe) bimodal nanovector as a platform for image-guided therapy, Inside Chem. 3 (2) (2017) 303–322.
[33] J. Liu, T. Liu, P. Du, L. Zhang, J. Lei, Metal-organic framework (MOF) hybrid as a tandem catalyst for enhanced therapy against hypoxic tumor cells, Angew. Chem. Int. Ed. 58 (23) (2019) 7808–7812.
[34] L. He, Q. Ni, J. Mu, W. Fan, L. Liu, Z. Wang, L. Li, W. Tang, Y. Liu, Y. Cheng, L. Tang, Z. Yang, Y. Liu, J. Zou, W. Yang, O. Jacobson, F. Zhang, P. Huang, X. Chen, Solvent-assisted self-assembly of a metal-organic framework based biocatalyst for cascade reaction driven photodynamic therapy, J. Am. Chem. Soc. 142 (14) (2020) 6822–6832.
[35] Q. Yang, Q. Xu, H.L. Jiang, Metal-organic frameworks meet metal nanoparticles: synergistic effect for enhanced catalysis, Chem. Soc. Rev. 46 (15) (2017) 4774–4808.
[36] G. Lu, S. Li, Z. Guo, O.K. Farha, B.G. Hauser, X. Qi, Y. Wang, X. Wang, S. Han, X. Liu, J.S. DuChene, H. Zhang, Q. Zhang, X. Chen, J. Ma, S.C. Loo, W.D. Wei, Y. Yang, J.T. Hupp, F. Huo, Imparting functionality to a metal-organic framework material by controlled nanoparticle encapsulation, Nat. Chem. 4 (4) (2012) 310–316.
[37] H. Liu, L. Chang, C. Bai, L. Chen, R. Luque, Y. Li, Controllable encapsulation of "clean" metal clusters within MOFs through kinetic modulation: towards advanced heterogeneous nanocatalysts, Angew. Chem. 55 (16) (2016) 5019–5023.
[38] J. Liang, K. Liang, Biocatalytic metal–organic frameworks: prospects beyond bioprotective porous matrices, Adv. Funct. Mater. 30 (27) (2020) 2001648.
[39] Q. Tang, S. Cao, T. Ma, X. Xiang, H. Luo, P. Borovskikh, R.D. Rodriguez, Q. Guo, L. Qiu, C. Cheng, Engineering biofunctional enzyme-mimics for catalytic therapeutics and diagnostics, Adv. Funct. Mater. 31 (7) (2020) 2007475.
[40] L. Ma, F.B. Jiang, X. Fan, L.Y. Wang, C. He, M. Zhou, S. Li, H.R. Luo, C. Cheng, L. Qiu, Metal-organic-framework-engineered enzyme-mimetic catalysts, Adv. Mater. 32 (49) (2020) 2003065.
[41] W. Xu, L. Jiao, Y. Wu, L. Hu, W. Gu, C. Zhu, Metal–organic frameworks enhance biomimetic cascade catalysis for biosensing, Adv. Mater. 33 (2021) 2005172.
[42] W. Cai, J. Wang, C. Chu, W. Chen, C. Wu, G. Liu, Metal-organic framework-based stimuli-responsive systems for drug delivery, Adv. Sci. 6 (1) (2019) 1801526.
[43] Y. Wang, J. Yan, N. Wen, H. Xiong, S. Cai, Q. He, Y. Hu, D. Peng, Z. Liu, Y. Liu, Metal-organic frameworks for stimuli-responsive drug delivery, Biomaterials 230 (2020) 119619.
[44] Y. Sun, L. Zheng, Y. Yang, X. Qian, T. Fu, X. Li, Z. Yang, H. Yan, C. Cui, W. Tan, Metal-organic framework nanocarriers for drug delivery in biomedical applications, Nano-Micro Lett. 12 (1) (2020) 103.
[45] X. Jiang, C. He, W. Lin, Supramolecular metal-based nanoparticles for drug delivery and cancer therapy, Curr. Opin. Chem. Biol. 61 (2021) 143–153.
[46] F. Demir Duman, R.S. Forgan, Applications of nanoscale metal-organic frameworks as imaging agents in biology and medicine, J. Mater. Chem. B 9 (16) (2021) 3423–3449.
[47] M.R. Shait Mohammed, V. Ahmad, A. Ahmad, S. Tabrez, H. Choudhry, M. A. Zamzami, M.A. Bakhrebah, A. Ahmad, S. Wasi, H. Mukhtar, M.I. Khan, Prospective of nanoscale metal organic frameworks [NMOFs] for cancer therapy, Semin. Cancer Biol. 69 (2021) 129–139.
[48] T. Sadhukha, T.S. Wiedmann, J. Panyam, Enhancing therapeutic efficacy through designed aggregation of nanoparticles, Biomaterials 35 (27) (2014) 7860–7869.
[49] R.J. White, R. Luque, V.L. Budarin, J.H. Clark, D.J. Macquarrie, Supported metal nanoparticles on porous materials. Methods and applications, Chem. Soc. Rev. 38 (2) (2009) 481–494.
[50] L. Guo, Y. Xu, A.R. Ferhan, G. Chen, D.H. Kim, Oriented gold nanoparticle aggregation for colorimetric sensors with surprisingly high analytical figures of merit, J. Am. Chem. Soc. 135 (33) (2013) 12338–12345.
[51] M. Aghayi-Anaraki, V. Safarifard, Fe_3O_4@MOF magnetic nanocomposites: synthesis and applications, Eur. J. Inorg. Chem. (2020) 1916–1937.
[52] Q. Yang, Y. Zhu, B. Luo, F. Lan, Y. Wu, Z. Gu, pH-responsive magnetic metal-organic framework nanocomposites for selective capture and release of glycoproteins, Nanoscale 9 (2) (2017) 527–532.
[53] J. Fang, Y. Yang, W. Xiao, B. Zheng, Y.B. Lv, X.L. Liu, J. Ding, Extremely low frequency alternating magnetic field-triggered and MRI-traced drug delivery by

optimized magnetic zeolitic imidazolate framework-90 nanoparticles, Nanoscale 8 (6) (2016) 3259–3263.
[54] J. Chen, J. Liu, Y. Hu, Z. Tian, Y. Zhu, Metal-organic framework-coated magnetite nanoparticles for synergistic magnetic hyperthermia and chemotherapy with pH-triggered drug release, Sci. Technol. Adv. Mater. 20 (1) (2019) 1043–1054.
[55] M. Xu, D. Li, K. Sun, L. Jiao, C. Xie, C. Ding, H.L. Jiang, Interfacial microenvironment modulation boosting electron transfer between metal nanoparticles and MOFs for enhanced photocatalysis, Angew. Chem. Int. Ed. 60 (30) (2021) 16372–16376.
[56] F. Ke, L.-G. Qiu, Y.-P. Yuan, X. Jiang, J.-F. Zhu, Fe_3O_4@MOF core–shell magnetic microspheres with a designable metal–organic framework shell, J. Mater. Chem. 22 (19) (2012) 9497.
[57] Y. Chen, Z. Xiong, L. Peng, Y. Gan, Y. Zhao, J. Shen, J. Qian, L. Zhang, W. Zhang, Facile preparation of core–shell magnetic metal–organic framework nanoparticles for the selective capture of phosphopeptides, ACS Appl. Mater. Interfaces 7 (30) (2015) 16338–16347.
[58] X. Wang, J. Xu, D. Yang, C. Sun, Q. Sun, F. He, S. Gai, C. Zhong, C. Li, P. Yang, Fe_3O_4@MIL-100(Fe)-UCNPs heterojunction photosensitizer: rational design and application in near infrared light mediated hypoxic tumor therapy, Chem. Eng. J. 354 (2018) 1141–1152.
[59] M. Zhao, K. Yuan, Y. Wang, G. Li, J. Guo, L. Gu, W. Hu, H. Zhao, Z. Tang, Metal-organic frameworks as selectivity regulators for hydrogenation reactions, Nature 539 (7627) (2016) 76–80.
[60] Z. Yuan, L. Zhang, S. Li, W. Zhang, M. Lu, Y. Pan, X. Xie, L. Huang, W. Huang, Paving metal-organic frameworks with upconversion nanoparticles via self-assembly, J. Am. Chem. Soc. 140 (45) (2018) 15507–15515.
[61] D. Feng, Z.Y. Gu, J.R. Li, H.L. Jiang, Z. Wei, H.C. Zhou, Zirconium-metalloporphyrin PCN-222: mesoporous metal-organic frameworks with ultrahigh stability as biomimetic catalysts, Angew. Chem. Int. Ed. 51 (41) (2012) 10307–10310.
[62] Y. Shen, T. Pan, L. Wang, Z. Ren, W. Zhang, F. Huo, Programmable logic in metal-organic frameworks for catalysis, Adv. Mater. 33 (2021) 2007442.
[63] L. Chen, Q. Xu, Metal-organic framework composites for catalysis, Matter 1 (1) (2019) 57–89.
[64] A. Paul, G. Vyas, P. Paul, D.N. Srivastava, Gold-nanoparticle-encapsulated ZIF-8 for a mediator-free enzymatic glucose sensor by amperometry, ACS Appl. Nano Mater. 1 (7) (2018) 3600–3607.
[65] J. Li, W. Liu, X. Wu, X. Gao, Mechanism of pH-switchable peroxidase and catalase-like activities of gold, silver, platinum and palladium, Biomaterials 48 (2015) 37–44.
[66] M. Comotti, C. Della Pina, R. Matarrese, M. Rossi, The catalytic activity of "naked" gold particles, Angew. Chem. Int. Ed. 43 (43) (2004) 5812–5815.
[67] D. Jiang, D. Ni, Z.T. Rosenkrans, P. Huang, X. Yan, W. Cai, Nanozyme: new horizons for responsive biomedical applications, Chem. Soc. Rev. 48 (14) (2019) 3683–3704.
[68] H.L. Jiang, B. Liu, T. Akita, M. Haruta, H. Sakurai, Q. Xu, Au@ZIF-8: CO oxidation over gold nanoparticles deposited to metal-organic framework, J. Am. Chem. Soc. 131 (32) (2009) 11302–11303.
[69] V. Lykourinou, Y. Chen, X.S. Wang, L. Meng, T. Hoang, L.J. Ming, R. L. Musselman, S. Ma, Immobilization of MP-11 into a mesoporous metal-organic framework, MP-11@mesoMOF: a new platform for enzymatic catalysis, J. Am. Chem. Soc. 133 (27) (2011) 10382–10385.
[70] Y.L. Liu, W.L. Fu, C.M. Li, C.Z. Huang, Y.F. Li, Gold nanoparticles immobilized on metal-organic frameworks with enhanced catalytic performance for DNA detection, Anal. Chim. Acta 861 (2015) 55–61.
[71] Q.L. Zhu, J. Li, Q. Xu, Immobilizing metal nanoparticles to metal-organic frameworks with size and location control for optimizing catalytic performance, J. Am. Chem. Soc. 135 (28) (2013) 10210–10213.
[72] N. Tsumori, L. Chen, Q. Wang, Q.L. Zhu, M. Kitta, Q. Xu, Quasi-MOF: exposing inorganic nodes to guest metal nanoparticles for drastically enhanced catalytic activity, Inside Chem. 4 (4) (2018) 845–856.
[73] Y.V. Kaneti, S. Dutta, M.S.A. Hossain, M.J.A. Shiddiky, K.L. Tung, F.K. Shieh, C. K. Tsung, K.C.-W. Wu, Y. Yamauchi, Strategies for improving the functionality of zeolitic imidazolate frameworks: tailoring nanoarchitectures for functional applications, Adv. Mater. 29 (38) (2017) 1700213.
[74] Y.H. Hu, H.J. Cheng, X.Z. Zhao, J.J. Wu, F. Muhammad, S.C. Lin, J. He, L. Q. Zhou, C.P. Zhang, Y. Deng, P. Wang, Z.Y. Zhou, S.M. Nie, H. Wei, Surface-enhanced Raman scattering active gold nanoparticles with enzyme-mimicking activities for measuring glucose and lactate in living tissues, ACS Nano 11 (6) (2017) 5558–5566.
[75] Y. Wang, M. Zhao, J. Ping, B. Chen, X. Cao, Y. Huang, C. Tan, Q. Ma, S. Wu, Y. Yu, Q. Lu, J. Chen, W. Zhao, Y. Ying, H. Zhang, Bioinspired design of ultrathin 2D bimetallic metal-organic-framework nanosheets used as biomimetic enzymes, Adv. Mater. 28 (21) (2016) 4149–4155.
[76] Y. Huang, M.T. Zhao, S.K. Han, Z.C. Lai, J. Yang, C.L. Tan, Q.L. Ma, Q.P. Lu, J. Z. Chen, X. Zhang, Z.C. Zhang, B. Li, B. Chen, Y. Zong, H. Zhang, Growth of Au nanoparticles on 2D metalloporphyrinic metal-organic framework nanosheets used as biomimetic catalysts for cascade reactions, Adv. Mater. 29 (2017) 1700102.
[77] J. Feng, H. Wang, Z. Ma, Ultrasensitive amperometric immunosensor for the prostate specific antigen by exploiting a Fenton reaction induced by a metal-organic framework nanocomposite of type Au/Fe-MOF with peroxidase mimicking activity, Microchim. Acta 187 (1) (2020) 95.
[78] X. Huang, M.A. El-Sayed, Gold nanoparticles: optical properties and implementations in cancer diagnosis and photothermal therapy, J. Adv. Res. 1 (1) (2010) 13–28.
[79] E.C. Abenojar, S. Wickramasinghe, J. Bas-Concepcion, A.C.S. Samia, Structural effects on the magnetic hyperthermia properties of iron oxide nanoparticles, Prog. Nat. Sci.: Met. Mater. Int. 26 (5) (2016) 440–448.
[80] W. Shang, C. Zeng, Y. Du, H. Hui, X. Liang, C. Chi, K. Wang, Z. Wang, J. Tian, Core-shell gold Nanorod@Metal-organic framework nanoprobes for multimodality diagnosis of glioma, Adv. Mater. 29 (2017) 1604381.
[81] L. Zhang, C. Liu, Y. Gao, Z. Li, J. Xing, W. Ren, L. Zhang, A. Li, G. Lu, A. Wu, L. Zeng, ZD2-Engineered gold Nanostar@Metal-organic framework nanoprobes for T_1 -weighted magnetic resonance imaging and photothermal therapy specifically toward triple-negative breast cancer, Adv. Healthcare Mater. 7 (24) (2018) 1801144.
[82] Y. Li, J. Jin, D. Wang, J. Lv, K. Hou, Y. Liu, C. Chen, Z. Tang, Coordination-responsive drug release inside gold nanorod@metal-organic framework core–shell nanostructures for near-infrared-induced synergistic chemo-photothermal therapy, Nano Res. 11 (6) (2018) 3294–3305.
[83] Y.C. Ma, Y.H. Zhu, X.F. Tang, L.F. Hang, W. Jiang, M. Li, M.I. Khan, Y.Z. You, Y. C. Wang, Au nanoparticles with enzyme-mimicking activity-ornamented ZIF-8 for highly efficient photodynamic therapy, Biomater. Sci. 7 (7) (2019) 2740–2748.
[84] J.Y. Zeng, M.K. Zhang, M.Y. Peng, D. Gong, X.Z. Zhang, Porphyrinic metal-organic frameworks coated gold nanorods as a versatile nanoplatform for combined photodynamic/photothermal/chemotherapy of tumor, Adv. Funct. Mater. 28 (8) (2018) 1705451.
[85] J. He, J. Dong, Y. Hu, G. Li, Y. Hu, Design of Raman tag-bridged core-shell Au@$Cu_3(BTC)_2$ nanoparticles for Raman imaging and synergistic chemo-photothermal therapy, Nanoscale 11 (13) (2019) 6089–6100.
[86] X. Han, J. Huang, X. Jing, D. Yang, H. Lin, Z. Wang, P. Li, Y. Chen, Oxygen-deficient black titania for synergistic/enhanced sonodynamic and photoinduced cancer therapy at near infrared-II biowindow, ACS Nano 12 (5) (2018) 4545–4555.
[87] X. Deng, S. Liang, X. Cai, S. Huang, Z. Cheng, Y. Shi, M. Pang, P. Ma, J. Lin, Yolk-shell structured Au Nanostar@Metal-organic framework for synergistic chemo-photothermal therapy in the second near-infrared window, Nano Lett. 19 (10) (2019) 6772–6780.
[88] M.T. Zhao, K. Yuan, Y. Wang, G.D. Li, J. Guo, L. Gu, W.P. Hu, H.J. Zhao, Z. Y. Tang, Metal-organic frameworks as selectivity regulators for hydrogenation reactions, Nature 539 (7627) (2016) 76–80.
[89] M. Zhao, K. Deng, L. He, Y. Liu, G. Li, H. Zhao, Z. Tang, Core-shell palladium Nanoparticle@Metal-organic frameworks as multifunctional catalysts for cascade reactions, J. Am. Chem. Soc. 136 (5) (2014) 1738–1741.
[90] H. Liu, L. Chang, C. Bai, L. Chen, R. Luque, Y. Li, Controllable encapsulation of "clean" metal clusters within MOFs through kinetic modulation: towards advanced heterogeneous nanocatalysts, Angew. Chem. Int. Ed. 55 (16) (2016) 5019–5023.
[91] X. Zhou, S. Guo, J. Gao, J. Zhao, S. Xue, W. Xu, Glucose oxidase-initiated cascade catalysis for sensitive impedimetric aptasensor based on metal-organic frameworks functionalized with Pt nanoparticles and hemin/G-quadruplex as mimicking peroxidases, Biosens. Bioelectron. 98 (2017) 83–90.
[92] H.Y. Chen, Q.M. Qiu, S. Sharif, S.N. Ying, Y.X. Wang, Y.B. Ying, Solution-phase synthesis of platinum nanoparticle-decorated metal-organic framework hybrid nanomaterials as biomimetic nanoenzymes for biosensing applications, ACS Appl. Mater. Interfaces 10 (28) (2018) 24108–24115.
[93] P. Ling, S. Cheng, N. Chen, C. Qian, F. Gao, Nanozyme-modified metal-organic frameworks with multienzymes activity as biomimetic catalysts and electrocatalytic interfaces, ACS Appl. Mater. Interfaces 12 (15) (2020) 17185–17192.
[94] X. Li, X. Li, D. Li, M. Zhao, H. Wu, B. Shen, P. Liu, S. Ding, Electrochemical biosensor for ultrasensitive exosomal miRNA analysis by cascade primer exchange reaction and MOF@Pt@MOF nanozyme, Biosens. Bioelectron. 168 (2020) 112554.
[95] Y.F. Liu, Y. Cheng, H. Zhang, M. Zhou, Y.J. Yu, S.C. Lin, B. Jiang, X.Z. Zhao, L. Y. Miao, C.W. Wei, Q.Y. Liu, Y.W. Lin, Y. Du, C.J. Butch, H. Wei, Integrated cascade nanozyme catalyzes in vivo ROS scavenging for anti-inflammatory therapy, Sci. Adv. 6 (29) (2020), eabb2695.
[96] Y. Zhang, F. Wang, C. Liu, Z. Wang, L. Kang, Y. Huang, K. Dong, J. Ren, X. Qu, Nanozyme decorated metal-organic frameworks for enhanced photodynamic therapy, ACS Nano 12 (1) (2018) 651–661.
[97] C. Liu, J. Xing, O.U. Akakuru, L.J. Luo, S. Sun, R.F. Zou, Z.S. Yu, Q.L. Fang, A. G. Wu, Nanozymes-engineered metal-organic frameworks for catalytic cascades-enhanced synergistic cancer therapy, Nano Lett. 19 (8) (2019) 5674–5682.
[98] Y. Li, Z. Di, J. Gao, P. Cheng, C. Di, G. Zhang, B. Liu, X. Shi, L.D. Sun, L. Li, C. H. Yan, Heterodimers made of upconversion nanoparticles and metal-organic frameworks, J. Am. Chem. Soc. 139 (39) (2017) 13804–13810.
[99] H.J. Cai, T.T. Shen, J. Zhang, C.F. Shan, J.G. Jia, X. Li, W.S. Liu, Y. Tang, A core-shell metal-organic-framework (MOF)-based smart nanocomposite for efficient NIR/H_2O_2-responsive photodynamic therapy against hypoxic tumor cells, J. Mater. Chem. B 5 (13) (2017) 2390–2394.
[100] J.B. DeCoste, M.H. Weston, P.E. Fuller, T.M. Tovar, G.W. Peterson, M.D. LeVan, O.K. Farha, Metal-organic frameworks for oxygen storage, Angew. Chem. Int. Ed. 53 (51) (2014) 14092–14095.
[101] Z. Xie, X. Cai, C. Sun, S. Liang, S. Shao, S. Huang, Z. Cheng, M. Pang, B. Xing, A.A. A. Kheraif, J. Lin, O_2-Loaded pH-responsive multifunctional nanodrug carrier for overcoming hypoxia and highly efficient chemo-photodynamic cancer therapy, Chem. Mater. 31 (2) (2018) 483–490.
[102] D.P. Ling, H.H. Li, W.S. Xi, Z. Wang, A. Bednarkiewicz, S.T. Dibaba, L.Y. Shi, L. N. Sun, Heterodimers made of metal-organic frameworks and upconversion

nanoparticles for bioimaging and pH-responsive dual-drug delivery, J. Mater. Chem. B 8 (6) (2020) 1316–1325.
[103] C. Hao, X. Wu, M. Sun, H. Zhang, A. Yuan, L. Xu, C. Xu, H. Kuang, Chiral core-shell upconversion nanoparticle@MOF nanoassemblies for quantification and bioimaging of reactive oxygen species in vivo, J. Am. Chem. Soc. 141 (49) (2019) 19373–19378.
[105] L. He, M. Brasino, C. Mao, S. Cho, W. Park, A.P. Goodwin, J.N. Cha, DNA-assembled core-satellite upconverting-metal-organic framework nanoparticle superstructures for efficient photodynamic therapy, Small 13 (24) (2017) 1700504.
[106] C. Liu, B. Liu, J. Zhao, Z. Di, D. Chen, Z. Gu, L. Li, Y. Zhao, Nd $^{3+}$ -sensitized upconversion metal-organic frameworks for mitochondria-targeted amplified photodynamic therapy, Angew. Chem. Int. Ed. 59 (7) (2020) 2634–2638.
[107] Z. Li, H. Gao, R. Shen, C. Zhang, L. Li, Y. Lv, L. Tang, Y. Du, Q. Yuan, Facet selectivity guided assembly of nanoarchitectures onto two-dimensional metal-organic-framework nanosheets, Angew. Chem. Int. Ed. 60 (2021) 17564–17569.
[108] Y. Shao, B. Liu, Z. Di, G. Zhang, L.D. Sun, L. Li, C.H. Yan, Engineering of upconverted metal-organic frameworks for near-infrared light-triggered combinational photodynamic/chemo-/immunotherapy against hypoxic tumors, J. Am. Chem. Soc. 142 (8) (2020) 3939–3946.
[109] Z. Li, X. Qiao, G. He, X. Sun, D. Feng, L. Hu, H. Xu, H.B. Xu, S. Ma, J. Tian, Core-satellite metal-organic framework@upconversion nanoparticle superstructures via electrostatic self-assembly for efficient photodynamic theranostics, Nano Res. 13 (12) (2020) 3377–3386.
[110] Y. Liu, Y. Yang, Y. Sun, J. Song, N.G. Rudawski, X. Chen, W. Tan, Ostwald ripening-mediated grafting of metal-organic frameworks on a single colloidal nanocrystal to form uniform and controllable MXF, J. Am. Chem. Soc. 141 (18) (2019) 7407–7413.
[111] F. Wang, Z. Li, X. Zhang, R. Luo, H. Hou, J. Lei, Transformable upconversion metal-organic frameworks for near-infrared light-programmed chemotherapy, Chem. Commun. 57 (63) (2021) 7826–7829.
[112] H. Zhang, C. Hao, A. Qu, M. Sun, L. Xu, C. Xu, H. Kuang, Heterostructures of MOFs and nanorods for multimodal imaging, Adv. Funct. Mater. 28 (48) (2018) 1805320.
[113] Z. Shi, K. Zhang, S. Zada, C. Zhang, X. Meng, Z. Yang, H. Dong, Upconversion nanoparticle-induced multimode photodynamic therapy based on a metal-organic framework/titanium dioxide nanocomposite, ACS Appl. Mater. Interfaces 12 (11) (2020) 12600–12608.
[114] Q. Wang, Y. Ji, J. Shi, L. Wang, NIR-driven water splitting H_2 production nanoplatform for H_2-mediated cascade-amplifying synergetic cancer therapy, ACS Appl. Mater. Interfaces 12 (21) (2020) 23677–23688.
[115] P. Guardia, R. Di Corato, L. Lartigue, C. Wilhelm, A. Espinosa, M. Garcia-Hernandez, F. Gazeau, L. Manna, T. Pellegrino, Water-soluble iron oxide nanocubes with high values of specific absorption rate for cancer cell hyperthermia treatment, ACS Nano 6 (4) (2012) 3080–3091.
[116] K.H. Bae, M. Park, M.J. Do, N. Lee, J.H. Ryu, G.W. Kim, C. Kim, T.G. Park, T. Hyeon, Chitosan oligosaccharide-stabilized ferrimagnetic iron oxide nanocubes for magnetically modulated cancer hyperthermia, ACS Nano 6 (6) (2012) 5266–5273.
[117] G. Salas, J. Camarero, D. Cabrera, H. Takacs, M. Varela, R. Ludwig, H. Dähring, I. Hilger, R. Miranda, M.d.P. Morales, F.J. Teran, Modulation of magnetic heating via dipolar magnetic interactions in monodisperse and crystalline iron oxide nanoparticles, J. Phys. Chem. C 118 (34) (2014) 19985–19994.
[118] G.C. Lavorato, R. Das, J. Alonso Masa, M.-H. Phan, H. Srikanth, Hybrid magnetic nanoparticles as efficient nanoheaters in biomedical applications, Nanoscale Adv. 3 (4) (2021) 867–888.
[119] L. Gao, J. Zhuang, L. Nie, J. Zhang, Y. Zhang, N. Gu, T. Wang, J. Feng, D. Yang, S. Perrett, X. Yan, Intrinsic peroxidase-like activity of ferromagnetic nanoparticles, Nat. Nanotechnol. 2 (9) (2007) 577–583.
[120] T. Kang, Y.G. Kim, D. Kim, T. Hyeon, Inorganic nanoparticles with enzyme-mimetic activities for biomedical applications, Coord. Chem. Rev. 403 (2020) 213092.
[121] C. Zhao, Z. Jiang, R. Mu, Y. Li, A novel sensor for dopamine based on the turn-on fluorescence of Fe-MIL-88 metal-organic frameworks-hydrogen peroxide-o-phenylenediamine system, Talanta 159 (2016) 365–370.
[122] Y. Zhang, W. Zhang, K. Chen, Q. Yang, N. Hu, Y. Suo, J. Wang, Highly sensitive and selective colorimetric detection of glutathione via enhanced Fenton-like reaction of magnetic metal organic framework, Sens. Actuators, B 262 (2018) 95–101.
[123] Y. Wu, Y. Ma, G. Xu, F. Wei, Y. Ma, Q. Song, X. Wang, T. Tang, Y. Song, M. Shi, X. Xu, Q. Hu, Metal-organic framework coated Fe_3O_4 magnetic nanoparticles with peroxidase-like activity for colorimetric sensing of cholesterol, Sens. Actuators, B 249 (2017) 195–202.
[124] N. Bagheri, A. Khataee, J. Hassanzadeh, B. Habibi, Sensitive biosensing of organophosphate pesticides using enzyme mimics of magnetic ZIF-8, Spectrochim. Acta, Part A 209 (2019) 118–125.
[125] X. Qian Tang, Y. Dan Zhang, Z. Wei Jiang, D. Mei Wang, C. Zhi Huang, Y. Fang Li, Fe_3O_4 and metal-organic framework MIL-101(Fe) composites catalyze luminol chemiluminescence for sensitively sensing hydrogen peroxide and glucose, Talanta 179 (2018) 43–50.
[126] A. Samui, A.R. Chowdhuri, T.K. Mahto, S.K. Sahu, Fabrication of a magnetic nanoparticle embedded NH_2-MIL-88B MOF hybrid for highly efficient covalent immobilization of lipase, RSC Adv. 6 (71) (2016) 66385–66393.
[127] J. Huo, J. Aguilera-Sigalat, S. El-Hankari, D. Bradshaw, Magnetic MOF microreactors for recyclable size-selective biocatalysis, Chem. Sci. 6 (3) (2015) 1938–1943.
[128] C. Hou, Y. Wang, Q. Ding, L. Jiang, M. Li, W. Zhu, D. Pan, H. Zhu, M. Liu, Facile synthesis of enzyme-embedded magnetic metal-organic frameworks as a reusable mimic multi-enzyme system: mimetic peroxidase properties and colorimetric sensor, Nanoscale 7 (44) (2015) 18770–18779.
[129] R. Zhai, Y.F. Yuan, F.L. Jiao, F.R. Hao, X. Fang, Y.J. Zhang, X.H. Qian, Facile synthesis of magnetic metal organic frameworks for highly efficient proteolytic digestion used in mass spectrometry-based proteomics, Anal. Chim. Acta 994 (2017) 19–28.
[130] S.L. Cao, H. Xu, L.H. Lai, W.M. Gu, P. Xu, J. Xiong, H. Yin, X.H. Li, Y.Z. Ma, J. Zhou, M.H. Zong, W.Y. Lou, Magnetic ZIF-8/cellulose/Fe_3O_4 nanocomposite: preparation, characterization, and enzyme immobilization, Bioresour. Bioprocess. 4 (1) (2017) 56.
[131] R. Ricco, P. Wied, B. Nidetzky, H. Amenitsch, P. Falcaro, Magnetically responsive horseradish peroxidase@ZIF-8 for biocatalysis, Chem. Commun. 56 (43) (2020) 5775–5778.
[132] C. Lin, K. Xu, R. Zheng, Y. Zheng, Immobilization of amidase into a magnetic hierarchically porous metal–organic framework for efficient biocatalysis, Chem. Commun. 55 (40) (2019) 5697–5700.
[133] B. Tan, H. Zhao, W. Wu, X. Liu, Y. Zhang, X. Quan, Fe_3O_4-AuNPs anchored 2D metal-organic framework nanosheets with DNA regulated switchable peroxidase-like activity, Nanoscale 9 (47) (2017) 18699–18710.
[134] S.-h. Noh, S.H. Moon, T.-H. Shin, Y. Lim, J. Cheon, Recent advances of magneto-thermal capabilities of nanoparticles: from design principles to biomedical applications, Nano Today 13 (2017) 61–76.
[135] S. Mourdikoudis, A. Kostopoulou, A.P. LaGrow, Magnetic nanoparticle composites: synergistic effects and applications, Adv. Sci. 8 (12) (2021) 2004951.
[136] M.R. Lohe, K. Gedrich, T. Freudenberg, E. Kockrick, T. Dellmann, S. Kaskel, Heating and separation using nanomagnet-functionalized metal-organic frameworks, Chem. Commun. 47 (11) (2011) 3075–3077.
[137] J. Lin, P. Xin, L. An, Y. Xu, C. Tao, Q. Tian, Z. Zhou, B. Hu, S. Yang, Fe3O4-ZIF-8 assemblies as pH and glutathione responsive T2-T1 switching magnetic resonance imaging contrast agent for sensitive tumor imaging in vivo, Chem. Commun. 55 (4) (2019) 478–481.
[138] S.K. Elsaidi, M.A. Sinnwell, D. Banerjee, A. Devaraj, R.K. Kukkadapu, T. C. Droubay, Z. Nie, L. Kovarik, M. Vijayakumar, S. Manandhar, M. Nandasiri, B. P. McGrail, P.K. Thallapally, Reduced magnetism in core-shell magnetite@MOF composites, Nano Lett. 17 (11) (2017) 6968–6973.
[139] S. Yu, J. Wan, K. Chen, A facile synthesis of superparamagnetic Fe_3O_4 supraparticles@MIL-100(Fe) core-shell nanostructures: preparation, characterization and biocompatibility, J. Colloid Interface Sci. 461 (2016) 173–178.
[140] H. Wang, Q. Chen, Y. Yu, K. Cheng, Y. Sun, Size- and solvent-dependent magnetically responsive optical diffraction of carbon-encapsulated superparamagnetic colloidal photonic crystals, J. Phys. Chem. C 115 (23) (2011) 11427–11434.
[141] D. Wang, J. Zhou, R. Chen, R. Shi, G. Xia, S. Zhou, Z. Liu, N. Zhang, H. Wang, Z. Guo, Q. Chen, Magnetically guided delivery of DHA and Fe ions for enhanced cancer therapy based on pH-responsive degradation of DHA-loaded Fe_3O_4@C@MIL-100(Fe) nanoparticles, Biomaterials 107 (2016) 88–101.
[142] M. He, J. Zhou, J. Chen, F. Zheng, D. Wang, R. Shi, Z. Guo, H. Wang, Q. Chen, Fe_3O_4@carbon@zeolitic imidazolate framework-8 nanoparticles as multifunctional pH-responsive drug delivery vehicles for tumor therapy *in vivo*, J. Mater. Chem. B 3 (46) (2015) 9033–9042.
[143] H. Zhang, Y.H. Li, Y. Chen, M.M. Wang, X.S. Wang, X.B. Yin, Fluorescence and magnetic resonance dual-modality imaging-guided photothermal and photodynamic dual-therapy with magnetic porphyrin-metal organic framework nanocomposites, Sci. Rep. 7 (2017) 44153.
[144] A. Lajevardi, M. Hossaini Sadr, M. Tavakkoli Yaraki, A. Badiei, M. Armaghan, A pH-responsive and magnetic Fe_3O_4@silica@MIL-100(Fe)/β-CD nanocomposite as a drug nanocarrier: loading and release study of cephalexin, New J. Chem. 42 (12) (2018) 9690–9701.
[145] X. Zhou, W. Zhao, M. Wang, S. Zhang, Y. Li, W. Hu, L. Ren, S. Luo, Z. Chen, Dual-modal therapeutic role of the lactate oxidase-embedded hierarchical porous zeolitic imidazolate framework as a nanocatalyst for effective tumor suppression, ACS Appl. Mater. Interfaces 12 (29) (2020) 32278–32288.
[146] M.X. Wu, J. Gao, F. Wang, J. Yang, N. Song, X. Jin, P. Mi, J. Tian, J. Luo, F. Liang, Y.W. Yang, Multistimuli responsive core-shell nanoplatform constructed from Fe_3O_4@MOF equipped with pillar[6]arene nanovalves, Small 14 (17) (2018) 1704440.
[147] A. Ray Chowdhuri, D. Bhattacharya, S.K. Sahu, Magnetic nanoscale metal organic frameworks for potential targeted anticancer drug delivery, imaging and as an MRI contrast agent, Dalton Trans. 45 (7) (2016) 2963–2973.
[148] H.X. Zhao, Q. Zou, S.K. Sun, C. Yu, X. Zhang, R.J. Li, Y.Y. Fu, Theranostic metal-organic framework core-shell composites for magnetic resonance imaging and drug delivery, Chem. Sci. 7 (8) (2016) 5294–5301.
[149] S.M. Dadfar, K. Roemhild, N.I. Drude, S. von Stillfried, R. Knuchel, F. Kiessling, T. Lammers, Iron oxide nanoparticles: diagnostic, therapeutic and theranostic applications, Adv. Drug Deliv. Rev. 138 (2019) 302–325.
[150] S.Y. Yin, G. Song, Y. Yang, Y. Zhao, P. Wang, L.M. Zhu, X. Yin, X.B. Zhang, Persistent regulation of tumor microenvironment via circulating catalysis of $MnFe_2O_4$@Metal–organic frameworks for enhanced photodynamic therapy, Adv. Funct. Mater. 29 (25) (2019) 1901417.
[151] X.Q. Qian, X.X. Han, L.D. Yu, T.M. Xu, Y. Chen, Manganese-based functional nanoplatforms: nanosynthetic construction, physiochemical property, and theranostic applicability, Adv. Funct. Mater. 30 (3) (2020) 1907066.

[152] W. Zhang, S. Li, X. Liu, C. Yang, N. Hu, L. Dou, B. Zhao, Q. Zhang, Y. Suo, J. Wang, Oxygen-generating MnO_2 nanodots-anchored versatile nanoplatform for combined chemo-photodynamic therapy in hypoxic cancer, Adv. Funct. Mater. 28 (13) (2018) 1706375.
[153] Z. Wang, X. Tang, X. Wang, D. Yang, C. Yang, Y. Lou, J. Chen, N. He, Near-infrared light-induced dissociation of zeolitic imidazole framework-8 (ZIF-8) with encapsulated CuS nanoparticles and their application as a therapeutic nanoplatform, Chem. Commun. 52 (82) (2016) 12210–12213.
[154] W. Jiang, H. Zhang, J. Wu, G. Zhai, Z. Li, Y. Luan, S. Garg, CuS@MOF-Based well-designed quercetin delivery system for chemo-photothermal therapy, ACS Appl. Mater. Interfaces 10 (40) (2018) 34513–34523.
[155] X. Ge, Z. Li, Q. Yuan, 1D ceria nanomaterials: versatile synthesis and bio-application, J. Mater. Sci. Technol. 31 (6) (2015) 645–654.
[156] D. Yu, M. Ma, Z. Liu, Z. Pi, X. Du, J. Ren, X. Qu, MOF-encapsulated nanozyme enhanced siRNA combo: control neural stem cell differentiation and ameliorate cognitive impairments in Alzheimer's disease model, Biomaterials 255 (2020) 120160.
[157] J. Liu, L.Y. Ye, W.H. Xiong, T. Liu, H. Yang, J. Lei, A cerium oxide@metal-organic framework nanoenzyme as a tandem catalyst for enhanced photodynamic therapy, Chem. Commun. 57 (22) (2021) 2820–2823.
[158] Y. Lv, D. Ding, Y. Zhuang, Y. Feng, J. Shi, H. Zhang, T.L. Zhou, H. Chen, R.J. Xie, Chromium-doped zinc Gallogermanate@Zeolitic imidazolate framework-8: a multifunctional nanoplatform for rechargeable in vivo persistent luminescence imaging and pH-responsive drug release, ACS Appl. Mater. Interfaces 11 (2) (2019) 1907–1916.
[159] H. Zhao, G. Shu, J. Zhu, Y. Fu, Z. Gu, D. Yang, Persistent luminescent metal-organic frameworks with long-lasting near infrared emission for tumor site activated imaging and drug delivery, Biomaterials 217 (2019) 119332.
[160] L.J. Chen, X. Zhao, Y.Y. Liu, X.P. Yan, Macrophage membrane coated persistent luminescence nanoparticle@MOF-derived mesoporous carbon core-shell nanocomposites for autofluorescence-free imaging-guided chemotherapy, J. Mater. Chem. B 8 (35) (2020) 8071–8083.
[161] Y.F. Meng, D.S. Zhang, X. Chen, Z.C. Dai, X.X. Yao, P. Cui, D.X. Yu, G.R. Zhang, X. W. Zheng, FePt nanoparticles embedded in metal-organic framework nanoparticles for tumor imaging and eradication, ACS Appl. Nano Mater. 3 (5) (2020) 4494–4503.
[162] J. Yao, Y. Liu, J. Wang, Q. Jiang, D. She, H. Guo, N. Sun, Z. Pang, C. Deng, W. Yang, S. Shen, On-demand CO release for amplification of chemotherapy by MOF functionalized magnetic carbon nanoparticles with NIR irradiation, Biomaterials 195 (2019) 51–62.
[163] C. Fang, D. Cen, Y. Wang, Y. Wu, X. Cai, X. Li, G. Han, ZnS@ZIF-8 core-shell nanoparticles incorporated with ICG and TPZ to enable H_2S-amplified synergistic therapy, Theranostics 10 (17) (2020) 7671–7682.
[164] Y.D. Zhu, S.P. Chen, H. Zhao, Y. Yang, X.Q. Chen, J. Sun, H.S. Fan, X.D. Zhang, PPy@MIL-100 nanoparticles as a pH- and near-IR-irradiation-responsive drug carrier for simultaneous photothermal therapy and chemotherapy of cancer cells, ACS Appl. Mater. Interfaces 8 (50) (2016) 34209–34217.
[165] Z. Tian, X. Yao, K. Ma, X. Niu, J. Grothe, Q. Xu, L. Liu, S. Kaskel, Y. Zhu, Metal-organic framework/graphene quantum dot nanoparticles used for synergistic chemo- and photothermal therapy, ACS Omega 2 (3) (2017) 1249–1258.
[166] R. Chen, J. Zhang, Y. Wang, X. Chen, J.A. Zapien, C.S. Lee, Graphitic carbon nitride Nanosheet@Metal-organic framework core-shell nanoparticles for photo-chemo combination therapy, Nanoscale 7 (41) (2015) 17299–17305.
[167] D. Wang, C. Zhao, G.Y. Gao, L.N. Xu, G.F. Wang, P.F. Zhu, Multifunctional $NaLnF_4$@MOF-ln nanocomposites with dual-mode luminescence for drug delivery and cell imaging, Nanomaterials 9 (9) (2019) 1274.
[168] S. Sene, M.T. Marcos-Almaraz, N. Menguy, J. Scola, J. Volatron, R. Rouland, J. M. Grenèche, S. Miraux, C. Menet, N. Guillou, F. Gazeau, C. Serre, P. Horcajada, N. Steunou, Maghemite-nanoMIL-100(Fe) bimodal nanovector as a platform for image-guided therapy, Inside Chem. 3 (2) (2017) 303–322.
[169] Z. Xue, M. Zhu, Y. Dong, T. Feng, Z. Chen, Y. Feng, Z. Shan, J. Xu, S. Meng, An integrated targeting drug delivery system based on the hybridization of graphdiyne and MOFs for visualized cancer therapy, Nanoscale 11 (24) (2019) 11709–11718.
[170] Y. Liu, C. Zhang, H. Liu, Y. Li, Z. Xu, L. Li, A. Whittaker, Controllable synthesis of up-conversion nanoparticles UCNPs@MIL-PEG for pH-responsive drug delivery and potential up-conversion luminescence/magnetic resonance dual-mode imaging, J. Alloys Compd. 749 (2018) 939–947.
[171] J.Y.R. Silva, Y.G. Proenza, L.L. da Luz, S. de Sousa Araujo, M.A.G. Filho, S. A. Junior, T.A. Soares, R.L. Longo, A thermo-responsive adsorbent-heater-thermometer nanomaterial for controlled drug release: (ZIF-8,Eu_xTb_y)@AuNP core-shell, Mater. Sci. Eng. C 102 (2019) 578–588.
[172] Y. You, D. Xu, X. Pan, X. Ma, Self-propelled enzymatic nanomotors for enhancing synergetic photodynamic and starvation therapy by self-accelerated cascade reactions, Appl. Mater. Today 16 (2019) 508–517.
[173] Y. Zhu, N. Xin, Z. Qiao, S. Chen, L. Zeng, Y. Zhang, D. Wei, J. Sun, H. Fan, Bioactive MOFs based theranostic agent for highly effective combination of multimodal imaging and chemo-phototherapy, Adv. Healthcare Mater. 9 (14) (2020) 2000205.
[174] Q. Chen, M. Xu, W. Zheng, T. Xu, H. Deng, J. Liu, Se/Ru-Decorated porous metal-organic framework nanoparticles for the delivery of pooled siRNAs to reversing multidrug resistance in taxol-resistant breast cancer cells, ACS Appl. Mater. Interfaces 9 (8) (2017) 6712–6724.
[175] A.R. Chowdhuri, D. Laha, S. Chandra, P. Karmakar, S.K. Sahu, Synthesis of multifunctional upconversion NMOFs for targeted antitumor drug delivery and imaging in triple negative breast cancer cells, Chem. Eng. J. 319 (2017) 200–211.
[176] V. Nejadshafiee, H. Naeimi, B. Goliaei, B. Bigdeli, A. Sadighi, S. Dehghani, A. Lotfabadi, M. Hosseini, M.S. Nezamtaheri, M. Amanlou, M. Sharifzadeh, M. Khoobi, Magnetic bio-metal-organic framework nanocomposites decorated with folic acid conjugated chitosan as a promising biocompatible targeted theranostic system for cancer treatment, Mater. Sci. Eng. C 99 (2019) 805–815.
[177] A.R. Chowdhuri, T. Singh, S.K. Ghosh, S.K. Sahu, Carbon dots embedded magnetic nanoparticles @chitosan @metal organic framework as a nanoprobe for pH sensitive targeted anticancer drug delivery, ACS Appl. Mater. Interfaces 8 (26) (2016) 16573–16583.
[178] S. Li, X. Shi, H. Wang, L. Xiao, A multifunctional dual-shell magnetic nanocomposite with near-infrared light response for synergistic chemo-thermal tumor therapy, J. Biomed. Mater. Res., Part B 109 (6) (2021) 841–852.
[179] P. Mukherjee, A. Kumar, K. Bhamidipati, N. Puvvada, S.K. Sahu, Facile strategy to synthesize magnetic upconversion nanoscale metal–organic framework composites for theranostics application, ACS Appl. Bio Mater. 3 (2) (2019) 869–880.
[180] H.-L. Cong, F.-F. Jia, S. Wang, M.-T. Yu, Y.-Q. Shen, B. Yu, Core–shell upconversion Nanoparticle@Metal–organic framework nanoprobes for targeting and drug delivery, Integrated Ferroelectrics Int. J. 206 (1) (2020) 66–78.
[181] X. Ke, N.Q. Qin, T. Zhang, F. Ke, X.Q. Yan, Highly augmented antioxidant and anticancer effect of biocompatible MIL-100(Fe)@SiO_2-immobilized green tea catechin, J. Inorg. Organomet. Polym. Mater. 30 (3) (2020) 935–942.
[182] Y. Wang, C. Hou, Y. Zhang, F. He, M.Z. Liu, X.L. Li, Preparation of graphene nano-sheet bonded PDA/MOF microcapsules with immobilized glucose oxidase as a mimetic multi-enzyme system for electrochemical sensing of glucose, J. Mater. Chem. B 4 (21) (2016) 3695–3702.
[183] J. Meng, X. Chen, Y. Tian, Z. Li, Q. Zheng, Nanoscale metal-organic frameworks decorated with graphene oxide for magnetic resonance imaging guided photothermal therapy, Chem. Eur J. 23 (69) (2017) 17521–17530.
[184] Q. Zhu, W. Zhuang, Y. Chen, Z. Wang, V.B. Hernandez, J. Wu, P. Yang, D. Liu, C. Zhu, H. Ying, Z. Zhu, Nano-biocatalysts of Cyt c@ZIF-8/GO composites with high recyclability via a de Novo approach, ACS Appl. Mater. Interfaces 10 (18) (2018) 16066–16076.
[185] Y. Guo, Q. Sun, F.G. Wu, Y. Dai, X. Chen, Polyphenol-containing nanoparticles: synthesis, properties, and therapeutic delivery, Adv. Mater. 33 (2021) 2007356.
[186] H. Ejima, J.J. Richardson, F. Caruso, Metal-phenolic networks as a versatile platform to engineer nanomaterials and biointerfaces, Nano Today 12 (2017) 136–148.
[187] L. Zhang, S.S. Wan, C.X. Li, L. Xu, H. Cheng, X.Z. Zhang, An adenosine triphosphate-responsive autocatalytic Fenton nanoparticle for tumor ablation with self-supplied H_2O_2 and acceleration of Fe(III)/Fe(II) conversion, Nano Lett. 18 (12) (2018) 7609–7618.
[188] B. Liu, H. Shioyama, T. Akita, Q. Xu, Metal-organic framework as a template for porous carbon synthesis, J. Am. Chem. Soc. 130 (16) (2008) 5390–5391.
[189] L. Huang, J. Chen, L. Gan, J. Wang, S. Dong, Single-atom nanozymes, Sci. Adv. 5 (5) (2019) eaav5490.
[190] S. Dang, Q.-L. Zhu, Q. Xu, Nanomaterials derived from metal–organic frameworks, Nat. Rev. Mater. 3 (2017) 17075.
[191] X.F. Lu, Y. Fang, D. Luan, X.W.D. Lou, Metal-organic frameworks derived functional materials for electrochemical energy storage and conversion: a mini review, Nano Lett. 21 (2021) 1555–1565.
[192] C. Wang, J. Kim, J. Tang, M. Kim, H. Lim, V. Malgras, J. You, Q. Xu, J. Li, Y. Yamauchi, New strategies for novel MOF-derived carbon materials based on nanoarchitectures, Inside Chem. 6 (1) (2020) 19–40.
[193] J. Zhao, W. Dong, X. Zhang, H. Chai, Y. Huang, FeNPs@Co_3O_4 hollow nanocages hybrids as effective peroxidase mimics for glucose biosensing, Sens. Actuators, B 263 (2018) 575–584.
[194] J.S. Mou, X.Z. Xu, F.F. Zhang, J.F. Xia, Z.H. Wang, Promoting nanozyme cascade bioplatform by ZIF-derived N-doped porous carbon nanosheet-based protein/bimetallic nanoparticles for tandem catalysis, ACS Appl. Bio Mater. 3 (1) (2020) 664–672.
[195] S. Wang, L. Shang, L. Li, Y. Yu, C. Chi, K. Wang, J. Zhang, R. Shi, H. Shen, G.I. N. Waterhouse, S. Liu, J. Tian, T. Zhang, H. Liu, Metal-organic-framework-derived mesoporous carbon nanospheres containing porphyrin-like metal centers for conformal phototherapy, Adv. Mater. 28 (38) (2016) 8379–8387.
[196] X. Pan, L. Bai, H. Wang, Q. Wu, H. Wang, S. Liu, B. Xu, X. Shi, H. Liu, Metal-organic-framework-derived carbon nanostructure augmented sonodynamic cancer therapy, Adv. Mater. 30 (23) (2018) 1800180.
[197] X. Pan, W. Wang, Z. Huang, S. Liu, J. Guo, F. Zhang, H. Yuan, X. Li, F. Liu, H. Liu, MOF-derived double-layer hollow nanoparticles with oxygen generation ability for multimodal imaging-guided sonodynamic therapy, Angew. Chem. Int. Ed. 59 (32) (2020) 13557–13561.
[198] Q. Wang, D.G. Niu, J.S. Shi, L.L. Wang, A three-in-one ZIFs-derived CuCo(O)/GOx@PCNs hybrid cascade nanozyme for immunotherapy/enhanced starvation/photothermal therapy, ACS Appl. Mater. Interfaces 13 (10) (2021) 11683–11695.
[199] W. Dong, Y. Zhuang, S. Li, X. Zhang, H. Chai, Y. Huang, High peroxidase-like activity of metallic cobalt nanoparticles encapsulated in metal–organic frameworks derived carbon for biosensing, Sens. Actuators, B 255 (2018) 2050–2057.
[200] J.-C. Shu, X.-Y. Yang, X.-R. Zhang, X.-Y. Huang, M.-S. Cao, L. Li, H.-J. Yang, W.-Q. Cao, Tailoring MOF-based materials to tune electromagnetic property for great microwave absorbers and devices, Carbon 162 (2020) 157–171.
[201] Z. Xiang, Y. Qi, Y. Lu, Z. Hu, X. Wang, W. Jia, J. Hu, J. Ji, W. Lu, MOF-derived novel porous Fe_3O_4@C nanocomposites as smart nanomedical platforms for

combined cancer therapy: magnetic-triggered synergistic hyperthermia and chemotherapy, J. Mater. Chem. B 8 (37) (2020) 8671–8683.
[202] W. Duan, S. Qiao, M. Zhuo, J. Sun, M. Guo, F. Xu, J. Liu, T. Wang, X. Guo, Y. Zhang, J. Gao, Y. Huang, Z. Zhang, P. Cheng, S. Ma, Y. Chen, Multifunctional platforms: metal-organic frameworks for cutaneous and cosmetic treatment, Inside Chem. 7 (2) (2021) 450–462.
[203] F.C. Lin, Y. Xie, T. Deng, J.I. Zink, Magnetism, ultrasound, and light-stimulated mesoporous silica nanocarriers for theranostics and beyond, J. Am. Chem. Soc. 143 (16) (2021) 6025–6036.

Further reading

[1] Lingyu Zhang, Shengnan Li, Xiangjun Chen, Tingting Wang, Lu Li, Zhongmin Su, Chungang Wang, Tailored surfaces on 2D material: UFO-like cyclodextrin-Pd nanosheet/metal organic framework Janus nanoparticles for synergistic cancer therapy, Adv. Funct. Mater. 28 (51) (2018), https://doi.org/10.1002/adfm.201803815, 1803815–1803815.